AD NUMBER

AD909527

LIMITATION CHANGES

TO:

Approved for public release; distribution is unlimited. Document partially illegible.

FROM:

Distribution authorized to U.S. Gov't. agencies only; Test and Evaluation; MAR 1973. Other requests shall be referred to Air Force Avionics Laboratory, AFAL/TEO, Wright-Patterson AFB, OH 45433. Document partially illegible.

AUTHORITY

afal ltr, 20 jan 1976

AFAL-TR-73-94

0.85 MICRON SOLID STATE LASER MATERIAL EVALUATION

E.P. Chicklis, R.C. Folweiler, C.S. Naiman, et al

TECHNICAL REPORT AFAL-TR-73-94

APRIL 1973

AIR FORCE AVIONICS LABORATORY · ELECTRONIC TECHNOLOGY DIVISION
AIR FORCE SYSTEMS COMMAND
Wright-Patterson Air Force Base, Ohio 45433

NOTICE

When Government drawings, specifications, or other data are used for any purpose other than in connection with a definitely related Government procurement operation, the United States Government thereby incurs no responsibility nor any obligation whatsoever; and the fact that the government may have formulated, furnished, or in any way supplied the said drawings, specifications, or other data, is not to be regarded by implication or otherwise as in any manner licensing the holder or any other person or corporation, or conveying any rights or permission to manufacture, use, or sell any patented invention that may in any way be related thereto.

Copies of this report should not be returned unless return is required by security considerations, contractual obligations, or notice on a specific document.

0.85 MICRON SOLID STATE LASER MATERIAL EVALUATION

E.P. Chicklis, R.C. Folweiler, C.S. Naiman, et al

FOREWORD

This is the first semi-annual report on Contract F33615-72-C-2065 and covers the work performed to evaluate the 0.85 micron solid state laser material Erbium:Yttrium Lithium Fluoride.

This contract is sponsored by Advanced Research Projects Agency under ARPA Order No. 2075. The amount of the contract is $155,270. The inclusive dates of the research reported are 5 June 1972 to 5 December 1972.

Mr. Richard L. Remski (TEO), Air Force Avionics Lab, Air Force Systems Command, Wright-Patterson Air Force Base, Ohio is the Project Monitor of this program.

These studies were carried out at Sanders Associates, Electro-Optics Division, Merrimack, New Hampshire 03060. Subcontracting services were provided by the Center of Material Sciences and Engineering, Crystal Physics Laboratory, Department of Electrical Engineering, Massachusetts Institute of Technology.

Dr. C.S. Naiman, Manager - Applied Physics Department is the Project Supervisor and E.P. Chicklis and R.C. Folweiler are the principal investigators. Mr. J.C. Doherty assisted with the laser measurements and Ms. S. Lichtensteiger the spectroscopic measurements. The subcontracting efforts were directed by Dr. A. Linz. Crystals were grown by Dr. D.R. Gabbe and R. Mills. Dr. H.P. Jenssen assisted with some of the spectroscopic measurements and analysis.

This technical report has been reviewed and is approved for publication.

Amos H. Dicke
Chief, Electro-Optics Device Br.
Electronic Technology Division

ABSTRACT

This first semi-annual report describes the current status of an investigation of Er:YLF as a 0.85 μm laser material operating at room temperature. Laser operation occurs via stimulated emission between the $^4S_{3/2}$-$^4I_{13/2}$ manifolds of the Er^{3+} ions. A description of the growth technique is presented. YLF crystals are grown by the Top Seeded Solution Technique, a modification of the Czochralski process. A compendium of the physical properties of the host material is presented including crystal structure, hardness, thermal conductivity, density, thermal expansion, and modulus of elasticity. Pump bands for the laser transition (at least to 0.360 μm) rapidly feed $^4S_{3/2}$ at a rate much faster than the decay rate of this state: 200 μs in 2% Er. The terminal state ($^4I_{13/2}$) lifetime is 13 ms and is strongly quenched with the addition of Pr^{3+} without appreciably perturbing $^4S_{3/2}$. Room temperature laser data includes pulsed thresholds as low as 4 joules with slope efficiencies up to 0.25%. Repetitively pulsed operation at 10 pps is reported.

TABLE OF CONTENTS

Section		Page
1	REPORT SUMMARY	1
2	INTRODUCTION	3
3	CRYSTAL GROWTH	5
3.1	Introduction	5
3.2	Crystal Chemistry	6
3.3	Materials Preparation	8
3.4	Crystal Growth	13
3.5	Equipment	13
3.6	Computer Control	17
3.7	Crystals Grown	19
4	MATERIAL CHARACTERIZATION	21
4.1	Crystal Structure	21
4.2	Hardness	22
4.3	Thermal Conductivity	22
4.4	Density	23
4.5	Thermal Expansion	23
4.6	Modulus of Elasticity and Strength	25
5	SPECTROSCOPY	31
5.1	$^4S_{3/2}$: The Initial State	31
5.1.1	Level Assignments	31
5.1.2	Fluorescence Lifetime	31
5.2	$^4I_{13/2}$: The Terminal Laser Level	37
5.2.1	Level Assignments	37
5.2.2	$^4I_{13/2}$ Fluorescence Lifetime	37

TABLE OF CONTENTS (Cont)

Section		Page
5.3	Pump Bands	38
5.4	Terminal State Quenching	39
5.4.1	Holmium (Ho^{3+})	39
5.4.2	Terbium (Tb^{3+})	40
5.4.3	Thulium (Tm^{3+})	40
5.4.4	Praeseodymium (Pr^{3+})	47
6	LASER MEASUREMENTS	51
6.1	Experimental Hardware	51
6.1.1	Pumping Cavities	51
6.1.2	Laser Rod Holders	51
6.1.3	Resonant Cavity	53
6.1.4	Radiometry	53
6.2	Laser Data	53
6.2.1	Rod 436.1: 2% Er-2% Ho (3 × 15 mm)	56
6.2.2	408A: 2% Er ($^4S_{3/2}$: 200 μs, $^4I_{13/2}$: 13 ms) 3 × 27 mm	56
6.2.3	Rod 437: 0.5% Er:YLF ($^4S_{3/2}$: 400 μs, $^4I_{13/2}$:13 ms) 3 × 15 mm	60
6.2.4	Rod 438.2: 2% Er:YLF 5 × 19 mm	60
6.2.5	Rod 438.1 (5 × 15 mm), Effects of Pulsewidth	60
6.2.6	Rod 446.1	62
6.2.7	Rod 408A (3 × 27 mm), Repetitively Pulsed Operation	62
6.3	Material Damage	65
	REFERENCES	67

LIST OF ILLUSTRATIONS

Figure		Page
3-1	Phase Diagram of $LiF-YF_3$ System	7
3-2	Diagram of Computer Controlled System for Fluoride Crystal Growth	18
4-1	Thermal Conductivity Apparatus	24
4-2	Linear Thermal Expansion of YLF	26
4-3	Thermal Expansion Coefficient for YLF	27
5-1	Energy Level Diagram of Er	32
5-2	Polarized Emission Spectra of 2% Er^{3+}:YLF	33
5-3	Multiphonon Relaxation Rates vs Energy Gap for $LaBr_3$, $LiYF_4$ and Y_2O_3	35
5-4	Er^{3+} Self Quenching	36
5-5	Er-Tm Resonant Transfer	41
5-6	Emission Spectrum of 2% Er:YLF	43
5-7	Emission Spectrum of 2% Er:1% Tm:YLF	44
5-8	Emission Spectrum of 2% Er:2% Tm:YLF	45
5-9	Accidental Resonances in Er-Tm:YLF	46
5-10	Emission Spectrum of 2% Er-1% Pr:YLF	48
5-11	Emission Spectrum of 2% Er-2% Pr:YLF	49
6-1	Laser Cavity	52
6-2	Energy Output vs Input of Er:YLF Rod #408	55
6-3	Energy Output vs Input of 2% Er-2% Ho:YLF Rod #436.1	57
6-4	Energy Output vs Input of 2% Er:YLF Rod #408A	59
6-5	Energy Output vs Input of 2% Er:YLF Rod #438.2	61
6-6	Input/Output vs Pulsewidth	63
6-7	Energy Output vs Input of 2% Er:YLF Rod #446.1	64

LIST OF TABLES

Table		Page
3-1	Mass Spectrographic Analyses of Four YF_3 Samples	11
3-2	Crystal Compositions Grown for This Program	19
4-1	X-Ray Measurements of Lattice Size	22
4-2	Knoop Hardness of YLF	22
4-3	Thermal Conductivity of YLF and Other Laser Hosts	23
4-4	Density of YLF	25
4-5	Linear Thermal Expansion of $a\beta$YLF	28
4-6	Modulus of Elasticity and Rupture	29
5-1	$^4S_{3/2}$ Energy Levels in YLF	31
5-2	$^4I_{13/2}$ Levels	38
5-3	Er:YLF Pump Bands	39
5-4	Quenching Effects of Tm^{3+} and Pr^{3+}:YLF	47
6-1	Summary of Previous Results	54
6-2	Long Pulse Input/Output	58

SECTION 1

REPORT SUMMARY

The results of the first six months of an eighteen month program to investigate the physical, spectroscopic, and laser properties of Er^{3+}:YLF are presented. Laser oscillations at 0.85 μm are obtained in this optically pumped solid state material as the result of stimulated $^4S_{3/2} - {}^4I_{13/2}$ transitions in the Er^{3+} ions. The objectives of this first phase of the program are:

a. Measurement of pertinent thermal and mechanical properties of this material.

b. Measurement of spectroscopic properties of interest with particular attention to quenching of the terminal state lifetime.

c. Measurement of the effects of variation of operating parameters (output coupling, pumping conditions) in low average power operation.

A detailed description of growth of YLF by the Top Seeded Solution technique is included in the text together with a discussion of the effects of the use of zone refined feed material. Modifications of the growth technique performed during this period are reported.

The crystal structure of YLF is the tetragonal Scheelite structure ($CaWO_4$) with a c/a of 2.08, and a density of 3.99 gm/cm^3 (undoped YLF). The thermal conductivity along the "a" axis orientation is 15×10^{-3} cal/cm-sec-^oC and the Knoop hardness 260 - 325 kg/mm^2. The thermal expansion coefficient along the "a" and "c" axes from -196 - 400^oC is reported together with modulus of elasticity, Poisson's ratio and the modulus of rupture.

Spectroscopic studies focussed on selecting co-dopants that would strongly quench terminal state of the laser transition ($^4I_{11/2}$) without affecting the storage time of the initial state. In 2% Er - 1% Pr:YLF the $^4I_{13/2}$ manifold

is quenched by a factor of 35; the $^4S_{3/2}$ lifetime is 170 μs. The terminal state lifetime of ~ 400 μs in this composition assures depopulation of the terminal state between pulses in moderate repetition rate operation (up to at least 30 pps).

Single shot laser measurements at room temperature were made with a variety of pumping conditions and different laser material compositions. The lowest threshold (4 joules) and highest slope efficiency (0.25%) have been obtained with 2% Er:YLF, the composition for which the highest optical quality rods were available. Repetitively pulsed operation (10 pps) has been demonstrated at room temperature. However, the output extinguishes after only ~ 40 - 50 pulses.

SECTION 2

INTRODUCTION

The erbium ion has provided a number of laser transitions including:

$^4I_{13/2} - {}^4I_{15/2}$ at 1.54 μm in various glasses first reported by Snitzer and Woodcock[1].

$^4I_{11/2} - {}^4I_{13/2}$ at 2.69 μm in CaF_2:(Er, Tm)F_3 reported by Robinson and Devor[2].

$^4S_{3/2} - {}^4I_{11/2}$ at 1.26 μm, and $^4S_{3/2} - {}^4I_{9/2}$ at ~1.7 in CaF_2 reported by Voronko et al[3].

Most recently Weber, Bass and Demars reported low pulsed threshold at 1.663 ($^4S_{3/2} - {}^4I_{9/2}$) in Er:$YAlO_3$ with a threshold of about 50 joules at room temperature[4].

The first report of the $^4S_{3/2} - {}^4I_{13/2}$ transition was by Goldstein and Mastrup[5] in CaF_2:(Er, Tm)F_3 at 77°K with a relatively high pulsed threshold. Later, Voronko[6] reported the laser transition in 4-8% Er^{3+}:CaF_2 at 77°K with a threshold of ~100 Joules.

Recently room temperature laser operation of the $^4S_{3/2} - {}^4I_{13/2}$ transition (λ = 0.85 μm) was obtained[7] in this laboratory using Er^{3+}:YLF with a pulsed threshold of ~10 joules. It is the purpose of this program to assess the potential of this material with respect to material quality, thermal and mechanical definition, laser related spectroscopic properties, and laser performance in order to define the material's capabilities and limitations.

SECTION 3
CRYSTAL GROWTH

3.1 INTRODUCTION

Crystals of $LiYF_4$ doped with Er, Er-Tm, and Er-Pr have been grown by the Top-Seeded Solution technique[8] in an atmosphere of highly purified helium. Much of the technology developed for the fluoride crystal program supports the synthesis of highly purified low oxide content fluoride starting materials (feed) and provides the experimental basis for growth under conditions of very low recontamination of high-quality single crystals. The purification means are hydrofluorination at elevated temperatures of commercial rare-earth fluorides, zone-refining of either REF_3 or $LiREF_4$ compounds, and crystallization-purification by Czochralski growth. Crystal growth is carried out in pressure and vacuum-tight furnaces (leak rate 10^{-9} std cc/sec of He, or better) which, along with the charge, is outgassed to 10^{-6} torr at elevated temperatures in preparation for a crystal growth run. The crystal growth is carried out in an atmosphere of He purified by passage through a quartz diffusion cell.

In the system $LiF-YF_3$, incongruently melting $LiYF_4$ crystallizes as the primary phase over the composition range 51 to 75 mol % LiF, and this behavior is unaffected by small amounts of rare-earth dopants. Crystals are nucleated on an 'a' axis $LiYF_4$ single crystal seed from melts containing 53 mol % LiF and the desired proportions of YF_3, ErF_3, and other dopants. To maintain stable, inclusion-free growth of a constant diameter boule, a combination of pulling and temperature lowering rates ranging between 1 - 2 mm/hour and 0.5 to 2°C/hour is used. These parameters require frequent readjustment during a growth run. Crystal rotation is essential as it provides some degree of melt stirring and rates between 40 and 60 rpm are used.

3.2 CRYSTAL CHEMISTRY

Phase diagrams for the systems LiF-REF_3 [9] and LiF-YF_3 [10] have been published and all of our experience indicates that these diagrams are correct. Figure 3-1 shows the LiF-YF_3 phase diagram. In the system LiF-YF_3 there is only one compound, $LiYF_4$, which melts incongruently at 819°C. The peritectic composition occurs at 49 mole % YF_3. The eutectic composition and temperature are 19 mole % YF_3 and 695°C, respectively. The systems LiF-REF_3 vary in character from a simple system with one eutectic through a system with one incongruent compound, $LiREF_3$, to a system with one congruently melting compound and two eutectics as the size of the rare earth ion decreases. The effect of $LiREF_4$ forming rare earth dopants on lattice parameters has not been observed accurately but is expected to be small as the dopant levels are low and their ionic radii do not vary much from that of yttrium. Even those rare earths which do not form a $LiREF_4$ phase (La, Ce, Pr, Nd and Sm) can be doped in small concentrations into the Y sites without effect on the crystal's structure or on its optical quality.

In those systems where $LiREF_4$ does form, it can be grown from a melt whose composition lies within the field bounded by the peritectic and eutectic or by the two eutectics. Our observations on systems LiF-YF_3-REF_3 made during crystal growth experiments show that substitution of as much as 50% of the Y by rare earths heavier than Sm alters the system very little, i.e., the melting point and incongruent behavior of $Li(Y,RE)F_4$ remain about the same. Since the $LiREF_4$ phase field occurs on the LiF-rich side of the incongruently melting compounds and predominantly on the LiF-rich side of the congruently melting one, all crystals are grown from LiF-rich melts.

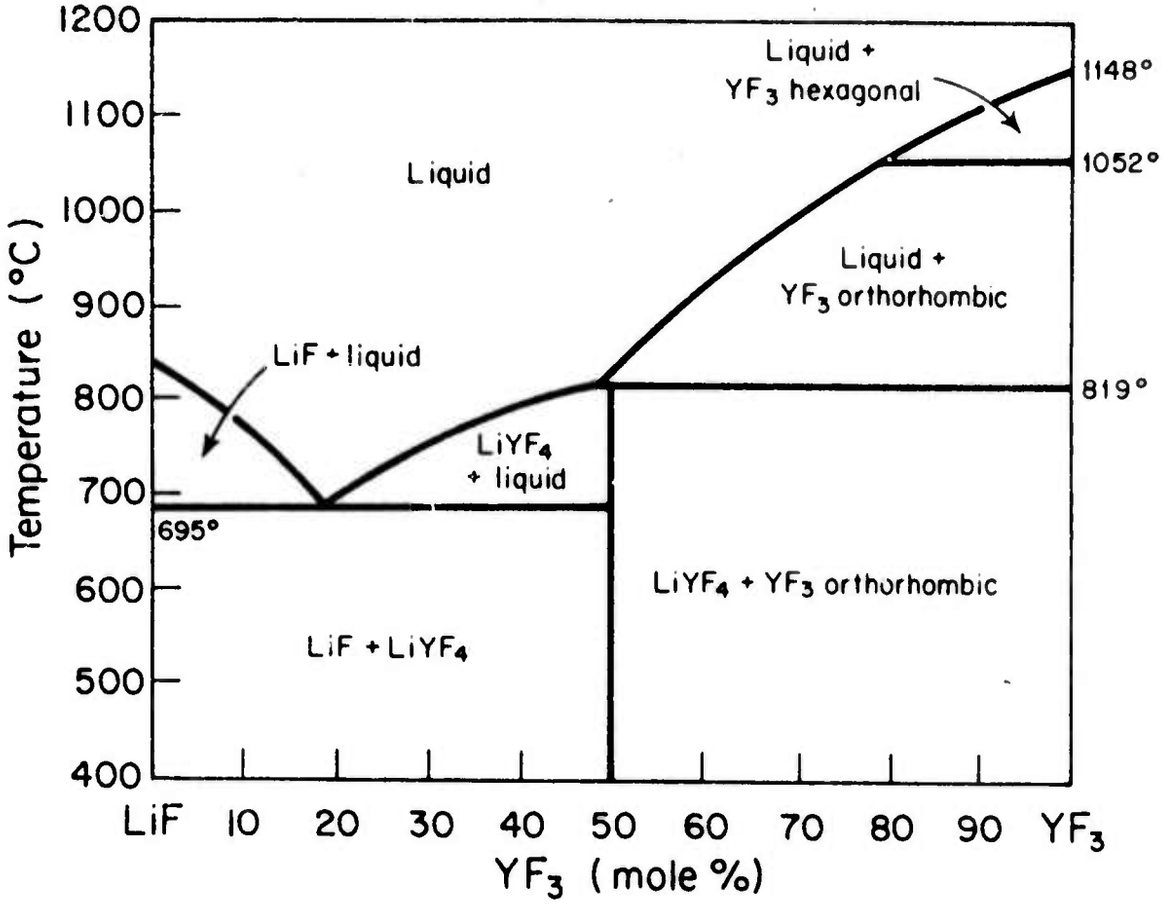

D-56

Figure 3-1 Phase Diagram of $LiF-YF_3$ System.

Little is known about the behavior of oxides in fluoride melts. Most experimental evidence suggests that some sort of oxide-fluoride phase is stable at very low oxide concentrations (possibly as low as 0.2 mol %) and that this phase either co-crystallizes with the fluoride phase during crystal growth or precipitates within the solid fluoride as it cools from the growth temperature to room temperature, and under conditions of excessive oxide contamination an opaque crystal is obtained. Therefore, preparation of low-oxide-content feed is of vital importance.

3.3 MATERIALS PREPARATION

The starting materials for the growth of Er:YLF are the parent compounds LiF, YF_3, ErF_3, and other REF_3 dopants. LiF is obtained from the Harshaw Chemical Company as single crystal chips and is used without further purification. Rare earth fluorides, as obtained from Research Chemicals, Inc. or Lindsay Rare Earths Div., Kerr-McGee, Inc., contain traces of moisture and oxides and must be treated in HF gas at 800°C and one atm pressure to be suitable for crystal growth feed. Mass spectrographic analysis of HF-treated rare earth fluorides indicates that the HF treatment can give a product containing between 75 and 150 ppm by weight of oxygen. The x-ray powder pattern of the HF-treated fluoride has much sharper diffraction lines and better resolution of $K\alpha_1$ and $K\alpha_2$ compared to the untreated fluoride. Some of this may be due to grain growth, but some water is also evolved from the "anhydrous" YF_3 during this treatment, resulting in the formation of a crystalline YF_3 from a gel-like $YF_3 \cdot XH_2O$.

The amounts of rare earth fluorides calculated to give the desired melt composition are weighed into a vitreous carbon boat and loaded into the hydrofluorination furnace. The weight of water evolved during drying is small and no correction of the fluoride weights to account for this loss is necessary. The system is purged with purified argon and the feed is first dried in flowing argon and then in flowing HF gas at 800°C over a five-hour period. The feed thus dried is transferred with minimum exposure to air to the crystal growing furnace.

Virtually all commercial fluorides (except for single crystal materials) are contaminated by organic compounds which cannot be washed out and which pyrolyze to carbon during hydrofluorination. Ultimately, this carbon appears on the melt surface where it interferes with seeding, causes nucleation of slightly misoriented grains, and often makes uncontrollable the diameter and shape of the growing crystal. Purification with respect to this residue is effected by trapping it on a preliminary crystal which is then removed from the furnace.

A dual-chamber furnace, which provides an interlock between the growth chamber and the atmosphere, permits removal of this crystal with its accumulated contaminants and replacement with a clean seed without having to shut down operations. This method, while effective, is cumbersome, sometimes requiring two successive applications before a clean melt surface is obtained. The cleaned melt is then ready for nucleation and growth of a laser rod boule. When spectroscopic samples are desired (i.e., 0.5 cm cubes), this cleaning procedure is not necessary as these insoluble contaminants do not affect the spectroscopic properties of the material.

Recently, zone-refining has been applied to the purification of rare earth fluorides. The objectives of this effort have been to further reduce the oxide content of the REF_3 materials, to remove other impurities as well, and to generate a well-crystallized, low-surface-area material which can be easily handled and stored without fear of recontamination.

The rare earth trifluorides are congruently melting, stable compounds and are therefore attractive candidates for zone-refining. But high temperature, destructive phase transition leaves the well crystallized material as millimeter and sub-millimeter pieces, which very nearly prevents visual evaluation of material quality through observation of color, grain size and clarity of the zone-refined product. This difficulty notwithstanding, zone-refining of REF_3 rather than $LiREF_4$ compounds was first investigated because many of the $LiREF_4$'s, especially $LiYF_4$, are incongruently melting.

Qualitative and semiquantitative data on zone-refined REF_3's obtained prior to the term of this contract are presented here to show the capabilities of zone-refining vis-a-vis fluoride purification[11].

YF_3, ErF_3 and TmF_3 have been zone refined. Typically 8 - 10 passes were made at rates of 3 - 4 cm per hour. Microscopic examination of samples of all the REF_3's taken along the length of the charges show:

a. Head of charge (pure end): clear material, no evidence of oxide precipitates - mm to sub-mm size crystallites.

b. Three quarters of total length from start: translucent material if the feed was not hydrofluorinated, clear if it was; only sub-mm size crystallites; a faint discoloration of the charge.

c. Last one-and-a-half inches of charge: heavily discolored; sometimes fluoresces while the rest of the charge does not; gives off an odor of hydrogen sulfide when acidified. Possible presence of a second phase, but this has not been verified.

This visual data suggests that impurities are being moved along with molten zone. Further verification of this was obtained via mass spectrographic analysis of a sample of zone-refined Research Chemicals, Inc. 99.99% YF_3. Four samples, identified below, were analyzed by E. B. Owens at MIT's Lincoln Laboratory under a joint fluoride purification program.

No. 1 HF dried, unrefined YF_3.
No. 2 Zone-refined YF_3, head of charge, HCl washed.
No. 3 Zone-refined YF_3, middle of charge, HCl washed.
No. 4 Zone-refined YF_3, end of charge, HCl washed.

Table 3-1 shows some of the data converted to concentration by weight.

The data indicate that zone refining has effected an overall purification. There are inconsistencies in some of the results (Er and Tm, for example), but

TABLE 3-1

CONCENTRATION IN PPM/WT OF YF_3

Element	Sample Number			
	1	2 (beginning)	3 (middle)	4 (end)
O	102	24	66	110
Na	22	2.6	2.3	16
Al	30	2.4	5.5	5.5
Si	3.7	1	1	1
Ca	6.3	1.6	3	8
Fe	42	5.7	5.3	15
La	0.9	ND	ND	5.7
Ce	0.7	ND	ND	3.8
Pr	1	ND	ND	12
Nd	2	ND	ND	24
Sm	7	ND	ND	185
Eu	ND	ND	ND	3
Gd	10	ND	ND	151
Tb	0.7	ND	ND	0.7
Dy	56	3	ND	19
Ho	ND	ND	0.8	1
Er	46	5	2	24
Tm	5	0.8	ND	5
Yb	59	ND	ND	166
Lu	0.8	ND	ND	ND
Ba	<8*	<8*	<8*	722

ND - Not Detected; < 0.5 ppm atomic

*No line appears for this element at the detection limit given here. Interference of the more abundant isotopes and/or the maximum exposure necessitates this change in detection limit.

experimental error is probably to blame. The HCl wash was used to clean the samples prior to analysis. Iron was removed in a preliminary HCl wash prior to zone refining, but after melting the charge.

A significant and very exciting result is the purification with respect to the rare earths. Reference to table 3-1 shows this to be general and very effective. The unrefined YF_3 has a total of 166 ppm atomic foreign rare earth atoms, while the purest zone-refined material has an impurity level of 8 ppm atomic. The impure end zone shows a total foreign rare earth content of 554 ppm atomic. Thus, purification by a factor of 12 - 20 has been achieved in the first zone; enrichment by a factor of 3 has been obtained in the end zone.

Incongruently melting $LiYF_4$ has also been zone refined. In one set of experiments LiF was added to the head of the charge after each pass to bring the initial melt into the $LiYF_4$ field. In other experiments $LiYF_4$ was repeatedly zone refined without addition of LiF. Results were similar for both experiments. The end of the charge, in this case $LiYF_4$-LiF eutectic mixture, was discolored, smelled of hydrogen sulfide when acidified and fluoresced under ultraviolet illumination.

In those runs where LiF was not added prior to each pass, the first inch of the charge was YF_3, but the loss of $LiYF_4$ to YF_3 over a 5 - 8 pass experiment, while reducing the yield of $LiYF_4$ is outweighed by the time saved by not adding LiF.

Both zone-refined $LiYF_4$ and YF_3 have been used as feed for crystals grown under this contract and a significant improvement in crystal quality over those grown from non-zone-refined feed has been achieved.

On occasion, single crystal chips of $LiYF_4$ remaining from previous growth experiments are used as feed. While purification by Czochralski crystallization is sound and quite effective, it is not regularly used because it sequesters the crystal-growing equipment.

Our fluoride purification technique then is to dry commercial REF_3 in HF-gas at 800°C and then zone-refine to effect further purification with respect to oxygen and cationic impurities. The beginning and middle portions of the zone-refined ingot are then selected for feed material.

3.4 CRYSTAL GROWTH

The furnaces are prepared for a crystal growth run by thorough cleaning, followed by degassing for several hours at 10^{-6} torr with the empty crucible at 1100°C. After this initial clean-up, the desired proportions of zone-refined feed and LiF are loaded, a seed mounted, and the furnace closed. A second outgassing to 450 - 500°C is performed and the furnace backfilled with purified He to a pressure of 4 psig.

When a laser boule is to be grown, the melt surface must be cleaned by growing a small crystal upon which is trapped all of the floating residue. A fresh seed is inserted via the interlock in the two-chamber furnace, and the growth run is commenced. Generally, growth of small samples for spectroscopic evaluation does not require preliminary cleaning of the melt surface.

Seeds are 5 x 5 x 15 mm 'a' axis pieces of pure $LiYF_4$ which have been cut from specially grown boules. Examination under the polarizing microscope permits selection of single grain material. A final seed-cleaning step, necessary to prevent recontamination of the cleaned melt surface, consists of polishing the seed with Syton*, followed by cleaning in hot aqueous HF, de-ionized water and careful drying in air. Growth is carried out with a constant seed rotation rate of 40 - 60 rpm, temperature lowering rates from 0.5 to 2°C/hour and pulling rates of 1 - 2 mm/hour.

3.5 EQUIPMENT

The furnaces consist of water-cooled stainless steel shells for ambient control, containing a graphite resistance heater, a graphite crucible support and pedestal shielded by molybdenum reflectors. The translatable and rotatable

*Trademark, Monsanto Corporation

water-cooled seed rod passes through a double-pumped integral 'O'-ring seal and bearing located at the top of the shell. All the seals are demountable and are made with Viton 'O' rings. Temperature is sensed with a Chromel-Alumel thermocouple. The oil diffusion pumps are capable of evacuating the furnaces of 10^{-6} torr with the crucible at 1100°C. The atmosphere is produced by passing commercial He through an Electron Technology Industries' diffusion cell. The mechanical system performance is evaluated with a standard ionization gauge and with a C. E. C. helium mass spectrometer. One of the two growth furnaces is equipped with a gate valve dividing it into two chambers. This valve functions as an interlock, allowing seeds and crystals - while attached to the seed rod - to be removed to the upper chamber and thence to the atmosphere and vice versa, without exposing the working volume to atmospheric contamination. This interchange operation is carried out with the furnace powered and the charge molten. The second furnace is now a single chamber unit and is being remodeled for two-chamber operation. Changing seeds can only be accomplished if the furnace is shutdown and opened, which prevents a completely clean melt surface from being obtained. Normally, therefore, this furnace is used only for the growth of spectroscopic samples. The zone refiner was specially built to handle fluorides and is described in Reference (11).

A crystal growth run takes on the average ten days, varying from eight to sixteen days, depending on the efficiency of each part of the operation. This includes, in order of execution:

1	clean up	
2.	outgassing minus charge	(1-2 days)
3.	leak detection	

4.	loading the charge	(1/2-2 1/2 days)
5.	outgassing the charge	
6.	leak detection if necessary	
7.	backfilling with purified He	
8.	melting the charge	
9.	melt clean up, trap floating scum on a growing crystal	(1/2-2 1/2 days)
10A.	remove contaminated boule, introduce new seed via dual chamber system	(1/4 day)
10B.	single chamber furnace - open, remove contaminated boule, install new seed, pumpdown, backfill, remelt	(1 day)
11.	seed melt contact	(1-2 days)
12.	growth to desired diameter	
13.	growth at 1-2 mm/hour to desired length	(3-6 days)
14.	cool to room temperature	(1 day)

These times are approximate and much depends upon how smoothly each operation goes and when the end of a work-day falls with respect to natural break points. Certain operations such as melt cleaning and seeding may have to be repeated to achieve satisfactory results.

The pulling phase takes three to six days. During this period, growth is interrupted several times by stopping the pulling and temperature lowering

program while retaining crystal melt contact. Introduction of severe optical defects at these points is a possibility due to sudden changes in growth conditions, but these defects - a very dense band of bubbles and inclusions - can be seen and eliminated by carefully controlled remelting without losing melt-crystal contact. Defects of low density do not correlate with interruptions in growth.

Growth is restarted by turning on the temperature lowering and pulling programs. Difficulties with diameter control arise because interruptions in the growth program change the steady state conditions and the operator's memorized, non-recordable understanding of how to manipulate the growth parameters, so that upon resumption of growth the next morning say, a few hours may be required to re-establish the correct combination of pulling and temperature lowering rates.

When one operator replaces another, and we have operated 18 to 24 hours per day schedules in the pulling mode, using two or three operators, a diameter variation is usually experienced as the new operator becomes accustomed to the growth requirements of that particular crystal run.

As pulling proceeds the operator needs to take corrective action to maintain a constant diameter. Usually the temperature lowering rate is adjusted and the pulling rate kept fixed. To achieve good diameter control under manual growth conditions the human operator must serve as a diameter sensor and also be able to apply some rate and reset action as he manipulates the pulling and temperature lowering rates. This is not really possible and at best the operator appears to act as an on-off controller with some proportioning action. With the very long system time constants that prevail when growing at 1 mm/hour diameter, the controlled variable oscillates in an irregular fashion. Under the best conditions, manual control is difficult and a crystal with varying diameter is obtained. Points of rapid diameter change often correspond to periods of high instantaneous

crystal growth rate which lead to optical and crystallographic inhomogeneities and limit the utility of the boule.

3.6 COMPUTER CONTROL

To overcome those problems generated by manual diameter control, i.e., poor diameter regulation resulting in degradation of optical quality, much less than 100% use of time during the pulling cycle (two or three shift operation is not too practical), and unfavorable geometry limiting the number of laser rods obtainable from a given boule, some form of automatic growth rate control is necessary for the consistent production of very high optical quality boules or YLF needed for lasers.

A closed loop digital control system which automatically controls the diameter and melt level at a constant pulling rate has been developed under a separate program[12] and is being applied to the NRC 2804 furnace. Although analog diameter control systems are available, none of them are sufficiently flexible for the problems encountered in a research operation where a wide range of different crystals are grown. A digital system based on a dedicated GRI-909 Model 40 computer offers both flexibility and the ability to control several growth systems at a time. A block diagram of the control system is shown in figure 3-2 The electro-optic sensors for melt level and crystal diameter control were developed to meet the special needs of a fluoride growth system, where the usual passive thermal sensing elements are not satisfactory, due to low temperatures and low emissivity. The diameter sensor observes the bright reflection from the meniscus between the growing crystal and the fluid melt while the melt level sensor observes the reflection from the melt surface. Pulsed GaAs diodes are used as light sources with dual element Si photoconductive detectors. These signals are fed through a multiplexer and analog to digital converter to the computer.

Temperature signals from the thermocouple are processed by a digital thermometer which transmits a BCD signal to the computer. Necessary

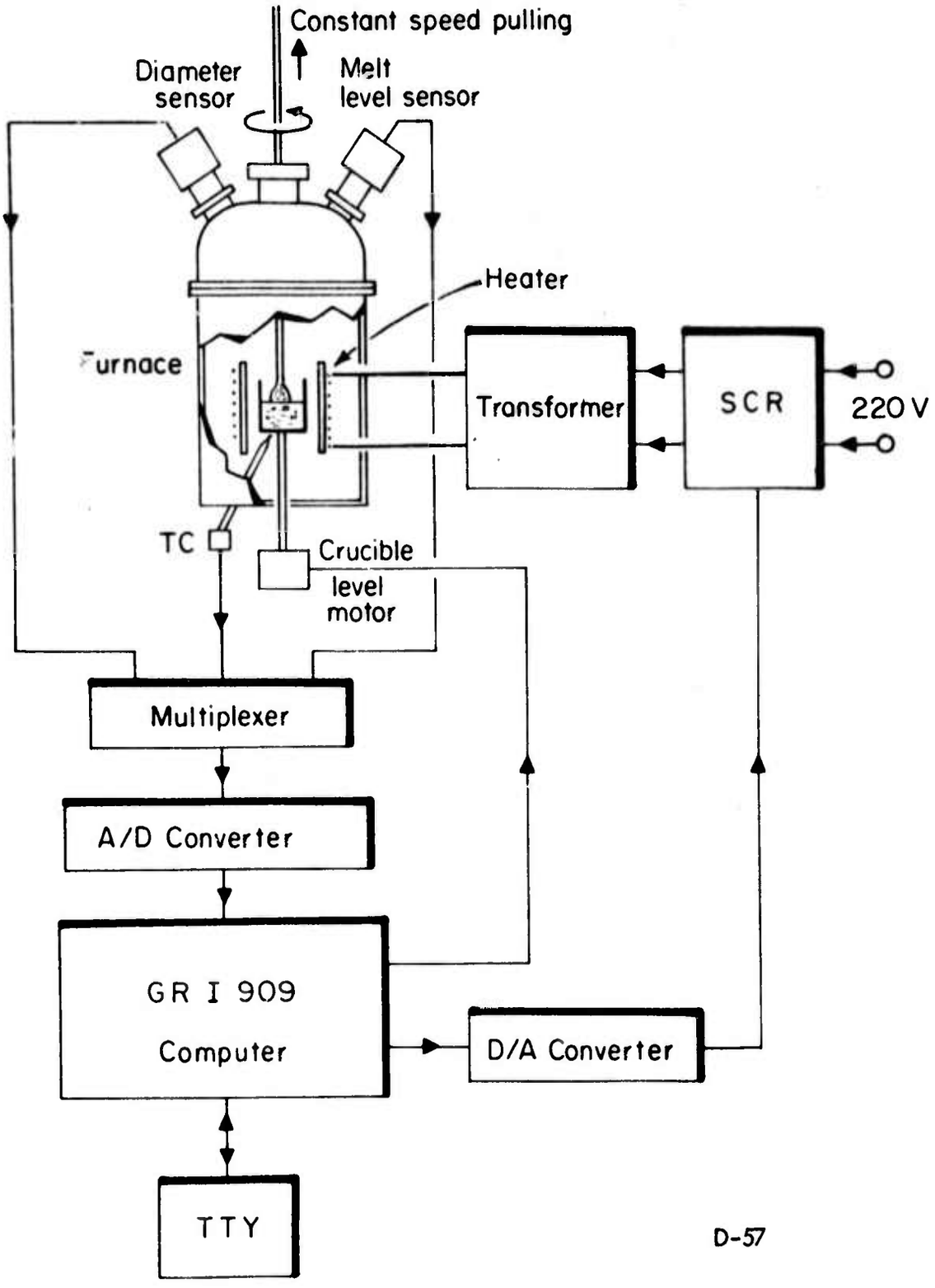

Figure 3-2 Diagram of Computer Controlled System For Fluoride Crystal Growth.

correction signals are sent directly to the crucible raising stepping motor, and the SCR power controller through a digital to analog converter.

It is expected that this system will enable us to grow fluoride crystals for laser rods of the highest possible optical quality. Strains and defects caused by operator inattention should be eliminated.

3.7 CRYSTALS GROWN

Table 3-2 lists the crystals that have been grown for this program.

TABLE 3-2

CRYSTAL COMPOSITIONS GROWN
FOR THIS PROGRAM

No.	Composition	Feed
177f	$LiYF_4$: Er 1%, Tm 1%	Zone refined $LiYF_4$, ErF_3, TmF_3
178f	$LiYF_4$: Er 2%, Tm 1%	Zone refined $LiYF_4$, ErF_3, TmF_3
180f	$LiYF_4$: 2% Er	Single crystal chips of $LiYF_4$: 2% Er
183f	$LiYF_4$: 2% Er, 1% Pr	Zone refined YF_3, ErF_3, PrF_3
184f	$LiYF_4$: 2% Er, 2& Pr	Zone refined YF_3, ErF_3, PrF_3
190f	$LiYF_4$: 1% Er	Zone refined $LiYF_4$, ErF_3
191f	$LiYF_4$: 1% Er, 2% Pr	Zone refined $LiYF_4$, ErF_3, PrF_3

Notes:

All LiF was Harshaw single crystal chips. Zone refined $LiYF_4$, YF_3, ErF_3 and TmF_3 were prepared from 99.99% Research chemical products. Zone refined PrF_3 was prepared from 99.9% Lindsay Rare Earths (formerly American Potash) material.

The single crystal chips used for crystal #180f were grown from 99.9% American Potash feed.

The crystal produced from zone-refined feed appeared to be of much better optical quality than those grown in the past from non-zone refined feed from the same source.

SECTION 4
MATERIAL CHARACTERIZATION

Many of the various material properties of doped and undoped $LiYF_4$ have been measured over a period of time. While not all of the property measurements reported herein were performed under this contract, a cumulative assembly of the known parameters is provided.

The tetragonal crystal structure of YLF requires that several of the properties be measured along specified crystalline axes. Where this is appropriate the measurements were performed on X-ray oriented samples. Additional measurements are either in progress under other programs, or are awaiting the availability of samples of adequate size or quality. Fabrication of laser rods has taken priority over property measurements in the past.

Earlier work[13] has indicated that there is no distinguishable difference between the optical phonon spectra of lightly doped YLF (2% Er and 2% Pr) and the phonon spectrum of heavily doped material ($LiErF_4$). This suggests that physical properties that depend on lattice vibration, such as thermal conductivity, will be little affected by composition, at least at room temperature. Thus, where measurements are not available for Er:YLF, values are presented for other compositions that should also represent this material. Certain property measurements, notably thermal conductivity, have been remeasured as better samples became available, and only the most recent data are reported.

4.1 CRYSTAL STRUCTURE

The crystal structure of $LiYF_4$ and all of its compositional analogs is the tetragonal Scheelite structure ($CaWO_4$), with a c/a ratio of 2.08. Other investigators have measured slightly different values of the unit cell, and are reported below in table 4-1 along with measurements made at MIT.

TABLE 4-1

X-RAY MEASUREMENTS OF LATTICE SIZE

ANGSTROM UNITS

Axis	MIT	Thoma, et al[10]	Keller[14]	Shand[15]
a	5.167	5.26	5.175	5.16
c	10.735	10.94	10.74	10.85

The effect of composition on lattice parameters has not been observed accurately, but is expected to be very minor since the rare earths used have very small variations in observed atomic radii from yttrium, the substitutional element in $LiYF_4$.

4.2 HARDNESS

The hardness of YLF is substantially less than the common crystalline laser hosts, ruby and yttrium aluminum garnet (YAG) and slightly less than Nd-doped laser glass. Values of hardness, reported in table 4-2 were measured by a Knoop indenter, using a standard load of 50 grams. The hardness values vary slightly with orientations, as is common in single crystals with the higher values observed at 45° to a <100> axis.

TABLE 4-2

KNOOP HARDNESS OF YLF (kg/mm^2)

Orientation	Pure YLF[11]	αβ-YLF[11]
(100)	260-325	260-350
(001)	260-325	280-320

4.3 THERMAL CONDUCTIVITY

An important property of any laser material that may be used at high repetition rate is thermal conductivity, especially in an application intended

for high average power. The value of thermal conductivity at room temperature has recently been remeasured in one orientation on a much better sample, table 4-3, in contrast to earlier measurements that were performed on a lower quality Nd-doped sample, full of bubbles and optical defects. The measurement reported here was made on a sample doped with 2% Er. An axial flow technique, depicted in figure 4-1, was used. Thermal conductivity, in units of cal cm^{-1}-sec^{-1}-$^{o}C^{-1}$, is reported in table 4-3, along with values for YAG, YAlO and FAP.

TABLE 4-3

THERMAL CONDUCTIVITY OF YLF AND OTHER LASER HOSTS

	($\times 10^{+3}$) cal/cm-sec-^{o}C)			
Orientation	YLF	YAG[16]	YAlO	FAP[16]
"a" axis	15	33	24	5.8
"b" axis			23	
"c" axis	NA			4.8

NA - not available

4.4 DENSITY

The material property parameter most strongly affected by composition is the density since the substitution of a much heavier rare earth ion for yttrium occurs with little measurable distortion of the lattice. Heavily doped materials, such as αβYLF, show very substantial differences in this parameter. The measurements reported in table 4-4 were made by immersion; X-ray measurements confirm the value observed for undoped YLF.

4.5 THERMAL EXPANSION

The thermal expansion of YLF was measured in the two principal directions, from -196 to 400^{o}C using a recording dilatometer. The temperature was allowed

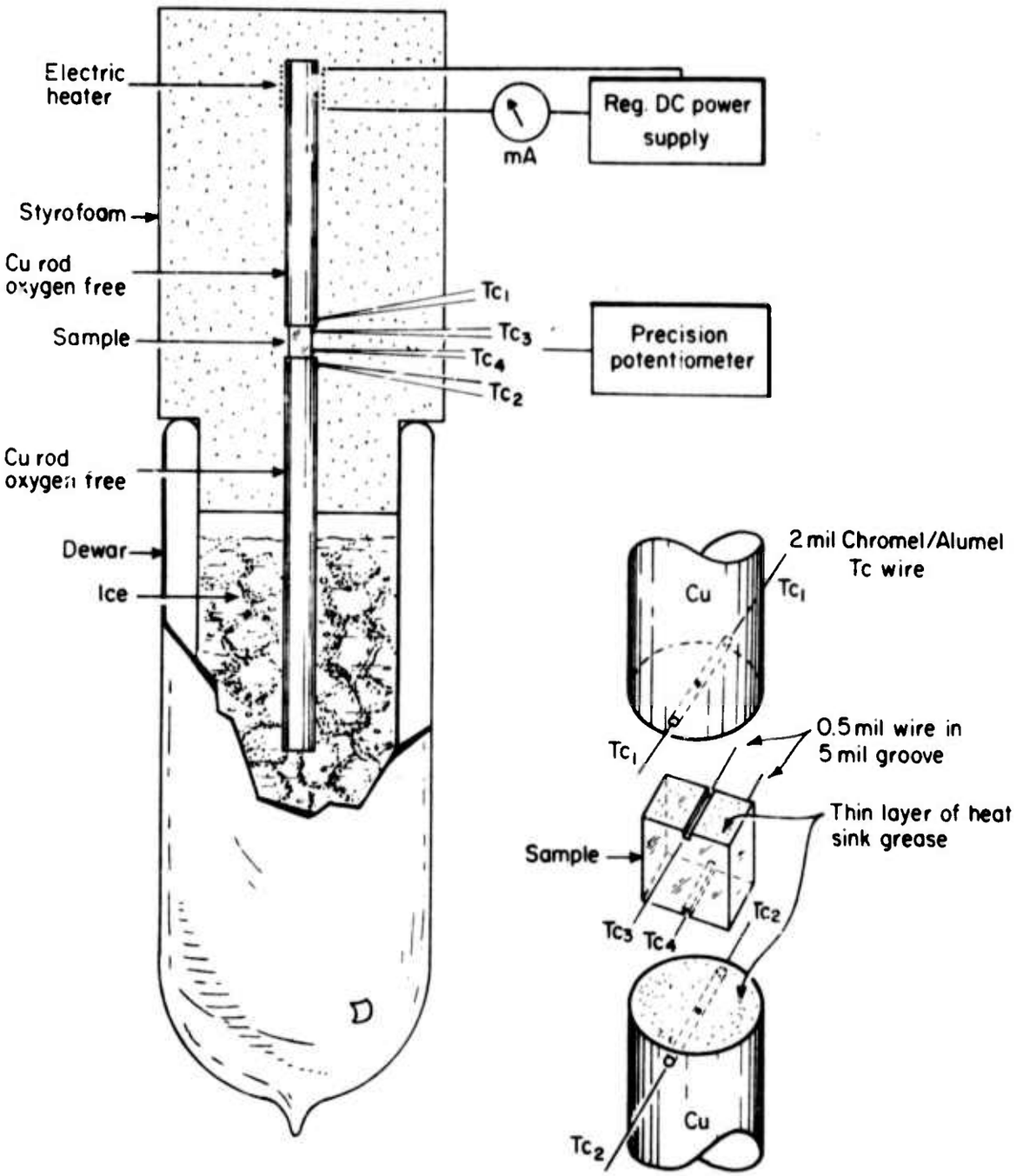

Figure 4-1 Thermal Conductivity Apparatus.

TABLE 4-4

DENSITY OF YLF

Material	Sample Number	Density (gm/cm^3)
2% Er:YLF	391	4.03
$\alpha\beta$YLF* [11]	360	5.07
2% Nd:YLF [11]	320	4.00
Undoped YLF [11]	253	3.99

* Composition $LiY_{0.32}Er_{0.55}Tm_{0.067}Yb_{0.05}Ho_{0.017}F_4$

to stabilize at each temperature before making the measurement. Values of expansion were computed based on the length of the sample measured at room temperature. A sample length of 45 mm was used for the "a" axis measurement. Table 3-5 and figure 4-2 present the observed values of thermal expansion. Figure 4-3 presents the instantaneous coefficient of thermal expansion, α, in Celsius units, computed over 50°C intervals.

4.6 MODULUS OF ELASTICITY AND STRENGTH

Strain gage techniques were used to measure Young's modulus, Poisson's ratio and the modulus of rupture of one 2% Er:YLF sample. Four point bending was used to load the specimen, which had a cross section of 0.19×0.16 inches, and was approximately 1.2 inches long. The ends of the bar were bonded to aluminum holders with epoxy to extend the sample length. Eastman 910 adhesive was used to bond the strain gages. Strain gages were applied to a pair of opposite surfaces to eliminate any question of axial loading, and a Poisson gage was used at right angles to each of the axial gages. This first set of gages was removed after completing the measurements and a new set applied to the remaining pair of surfaces and the specimen loaded in this second direction.

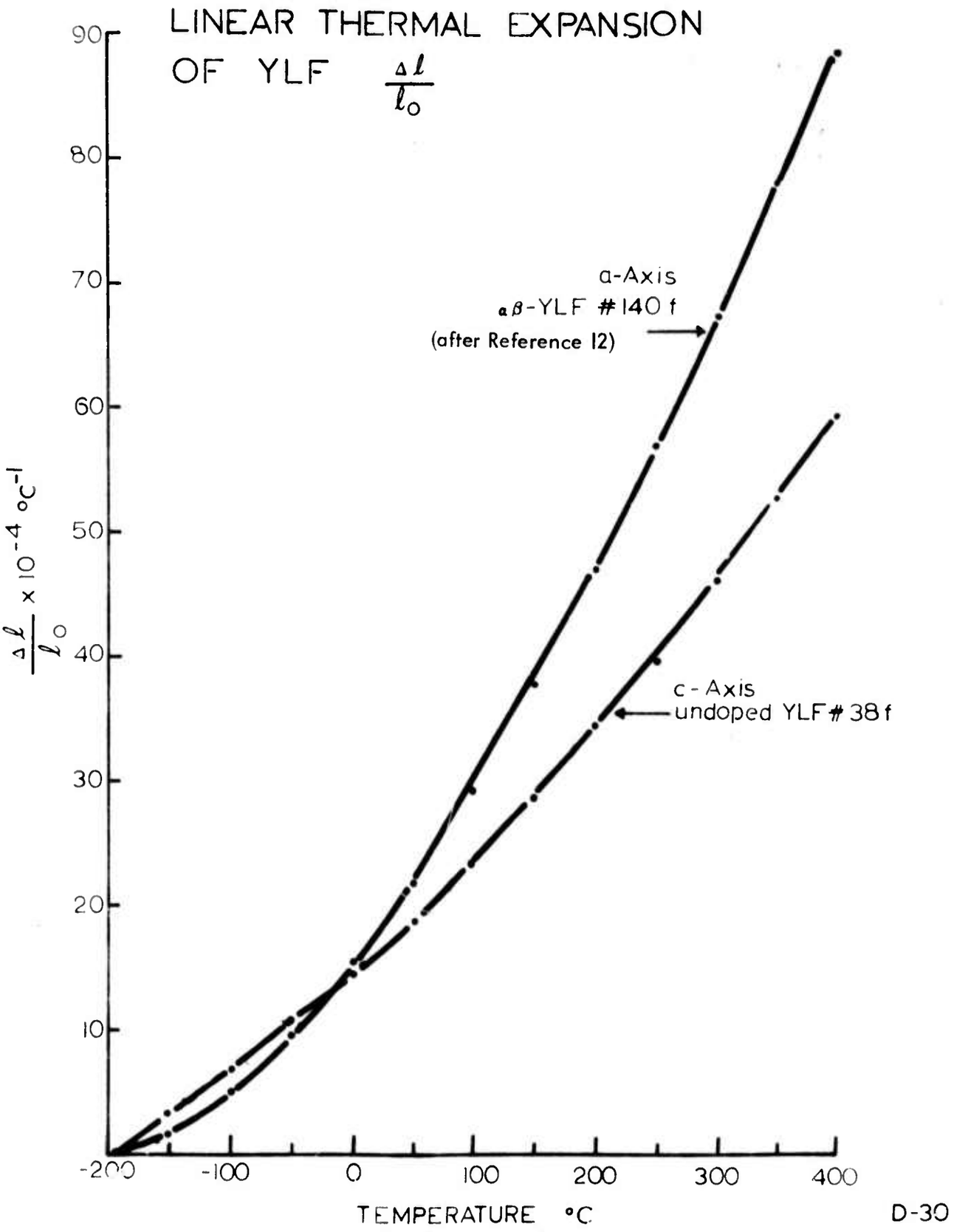

Figure 4-2 Linear Thermal Expansion of YLF.

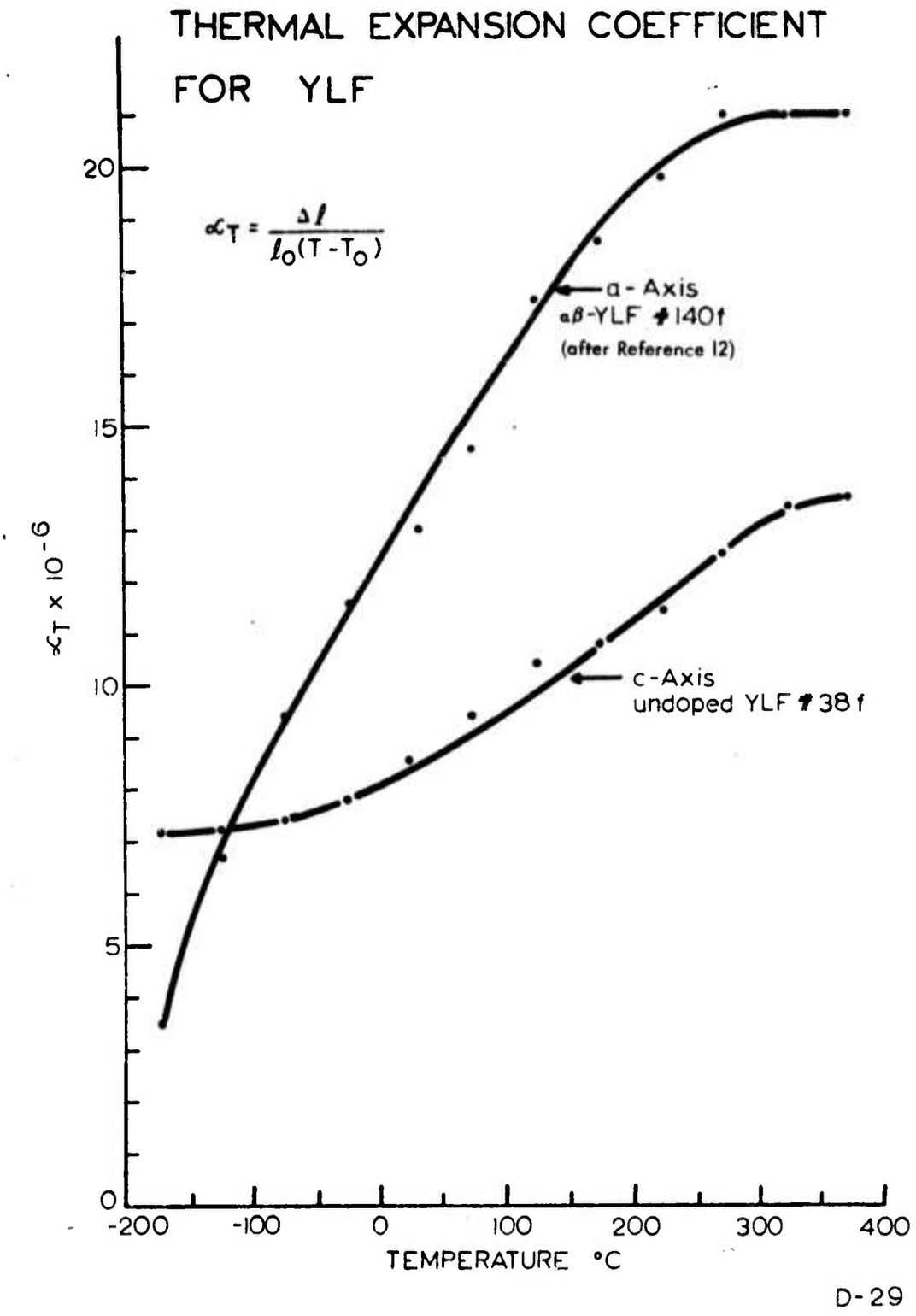

Figure 4-3 Thermal Expansion Coefficient for YLF.

TABLE 4-5

LINEAR THERMAL EXPANSION OF αβYLF

Temperature (°C)	$\Delta L/L_o \times 10^4$	
	"a" Axis[12]	"c" Axis
-196	0	0
-150	1.5	3.3
-100	4.8	6.9
- 50	9.5	10.6
0	15.3	14.5
50	21.8	18.8
100	29.1	23.5
150	37.8	28.7
200	47.1	34.1
250	57.0	39.8
300	67.5	46.1
350	78.0	52.8
400	88.5	59.6
Estimated Error:	±0.2	±0.3

The modulus of rupture test was performed in only one direction because it is destructive. As-sawn surfaces were present on two surfaces, while a partial polish was present on the two other surfaces. Sufficient imperfections were present in all surfaces to provide numerous stress concentrations, that the true fracture strength may be substantially higher.

The long sample axis was in the "a" direction of the tetragonal crystal, such that the gages were applied to both an "a" plane, a 100 surface, and a "c" plane, the (001) surface, for the two tests. The results for the one sample tested are shown in table 4-6.

TABLE 4-6

MODULUS OF ELASTICITY, RUPTURE AND POISSON'S RATIO

Sample: 180f, 2% Er:YLF		Surface	
		{100}	(001)
Modulus of Elasticity	Msi	11.6 ± 0.4	10.9 ± 0.4
	kg/mm^2	8190 ± 280	7680 ± 280
Poisson's Ratio		0.33 ± 0.04	0.33 ± 0.02
Modulus of Rupture	psi	3200 ± 80	Not measured
	kg/mm^2	2.25 ± 0.05	Not measured

SECTION 5
SPECTROSCOPY

The energy level diagram of Er^{3+} is shown in figure 5-1 including states up to $^2G_{7/2}$. The key states affecting laser operation are discussed below.

5.1 $^4S_{3/2}$: THE INITIAL STATE

5.1.1 LEVEL ASSIGNMENTS

In S_4 symmetry a J = 3/2 level splits into two Stark components. The measured positions of these levels in YLF are shown below.

TABLE 5-1

$^4S_{3/2}$ ENERGY LEVELS IN YLF

(from Reference (17))

Notation	Wavelength (μm)	Energy (cm^{-1})
E-1	0.542492	18433.5
E-2	0.540725	18493.7

The polarized room temperature emission spectrum of the $^4S_{3/2}$-$^4I_{13/2}$ transitions in a 2% Er:YLF sample is shown in figure 5-2. The linewidth of the transition centered at 0.8500 is ~8 cm^{-1}. This is the only transition which has been positively identified in the laser emission.

5.1.2 FLUORESCENCE LIFETIME

The fluorescence lifetime of this level is concentration and temperature dependent. In dilute samples (0.5-2% Er) at low temperature (4°K) the lifetime is 600 ± 30 μs[13]. As the measured multiphonon relaxation rate to $^4F_{9/2}$ is ~200 sec^{-1} (the multiphonon relaxation rate vs energy gap for YLF[13], $LaBr_3$[18]

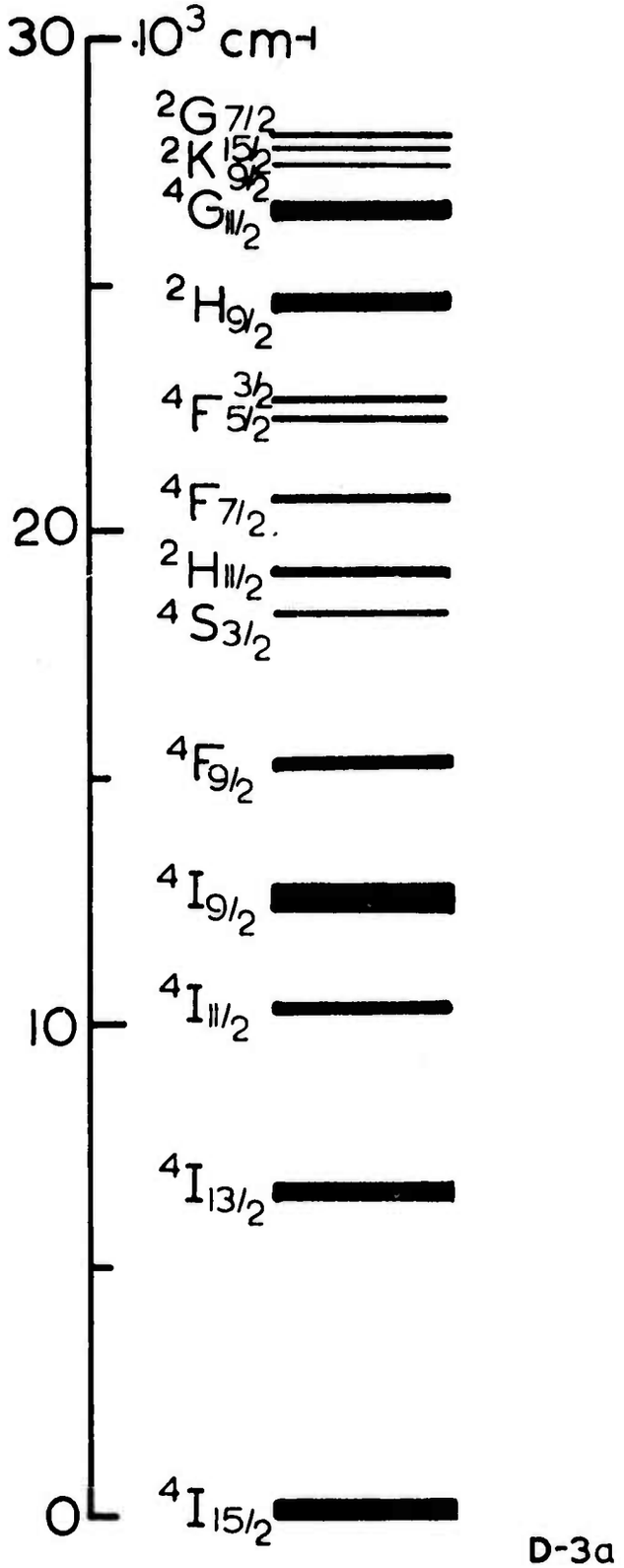

Figure 5-1 Energy Level Diagram of Er.

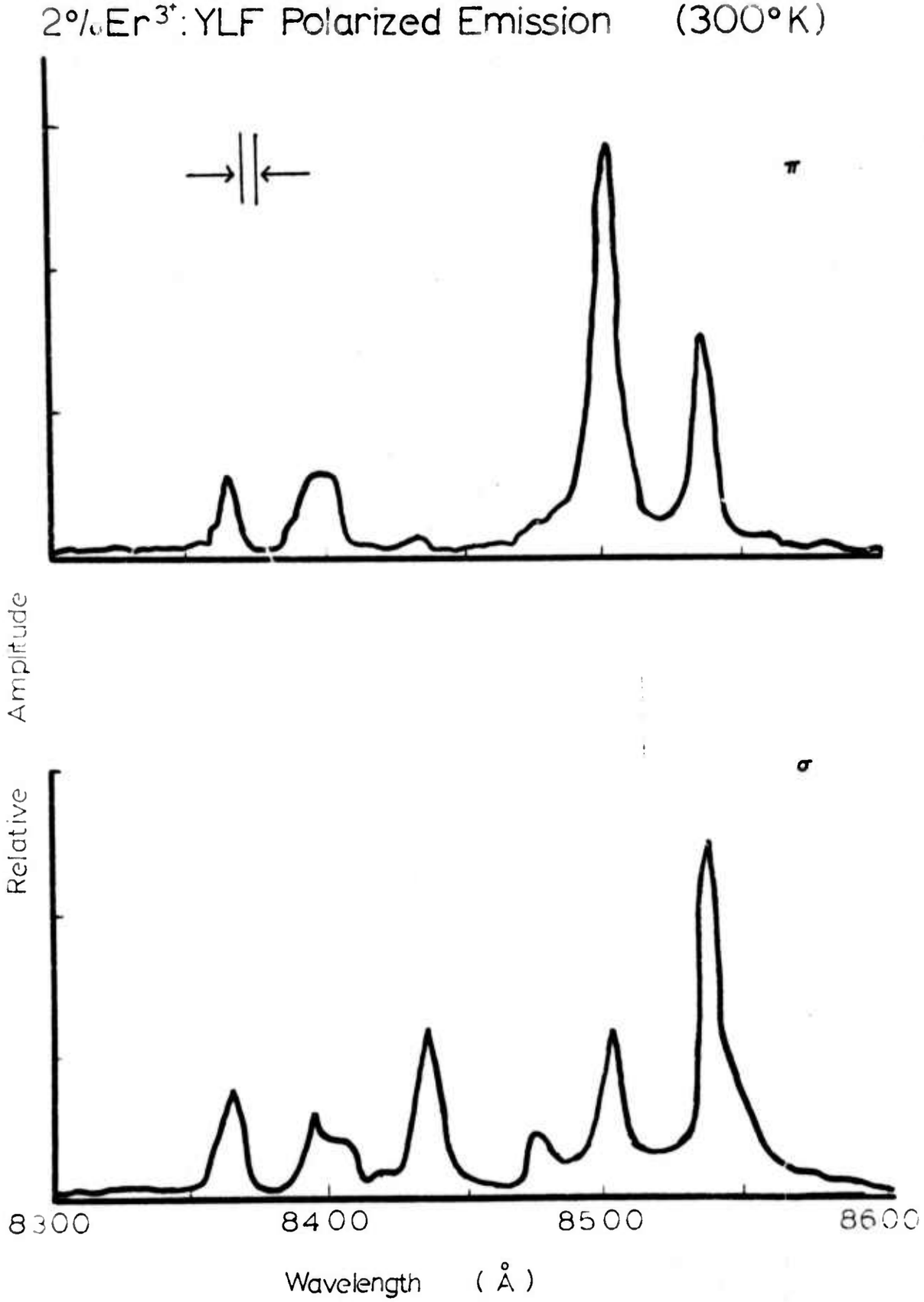

Figure 5-2 Polarized Emission Spectra of 2% Er^{3+}:YLF.

and Y_2O_3[18] is shown in figure 5-3), 600 μs is very nearly the radiative lifetime of this level. At room temperature the measured lifetimes are 0.5%: 400 μs, 2%: 200 μs, 5%: ~50 μs.

The observed concentration and temperature "quenching" of the $^4S_{3/2}$ manifold is believed to occur via resonant transfer between Er^{3+} ions. In this model (first proposed by Bakradze[19] to explain $^4S_{3/2}$ concentration quenching in Er:YAG) relaxation out of this state occurs via:

$^4S_{3/2}$-$^4S_{13/2}$ in one ion with simultaneous excitation of $^4I_{15/2}$-$^4I_{9/2}$ in another ion, and/or

$^4S_{3/2}$-$^4I_{9/2}$ in one ion with simultaneous excitation of $^4I_{15/2}$-$^4I_{13/2}$ in another ion.

In Er:YLF these transitions are very nearly resonant as indicated in figure 5-4 provided the upper states of the ground manifold are populated. Note that both transfers (A, B and C, D) initiate from the highest states of the ground ($^4I_{15/2}$) manifold, the energy decrement (A - B, C - D) increasing for lower lying levels of $^4I_{15/2}$.

By considering only the states for which A, B and C, D are nearly resonant, i.e., only the higher lying states of $^4I_{15/2}$, the number/sec of ions relaxing in this manner, $\dot{N}$, can be expressed as

$$\dot{N} = \frac{\omega N^S N^I}{N} \quad \text{(ions/sec)}$$

where

N^S = number density of ions in the upper level of $^4S_{3/2}$

N^I = number density of occupied states in highest levels of the ground manifold

ω = probability/sec for the transfer process assumed temperature and concentration independent

N = total number of ions

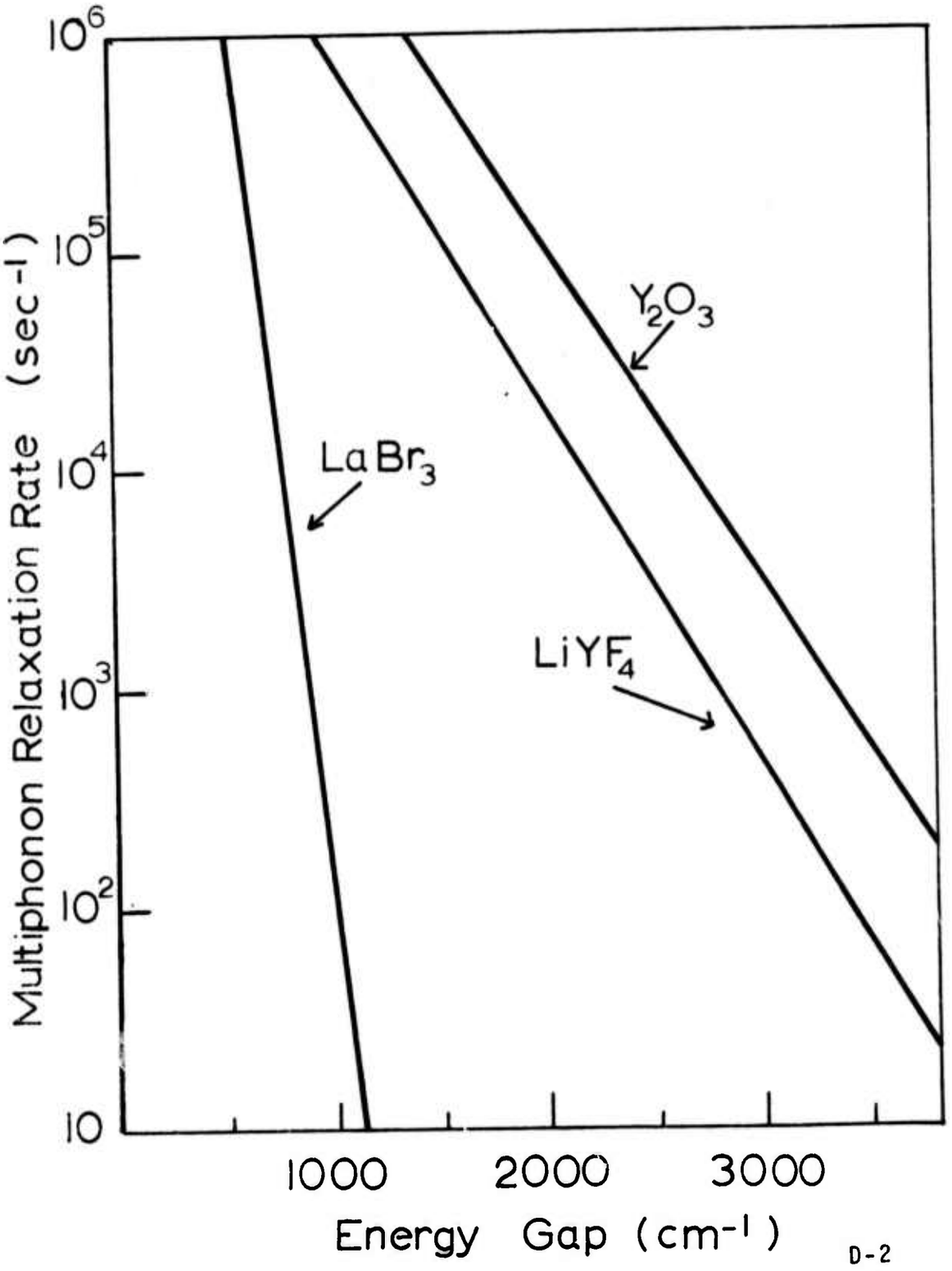

Figure 5-3 Multiphonon Relaxation Rates vs. Energy Gap For $LaBr_3$, $LiYF_4$ and Y_2O_3.

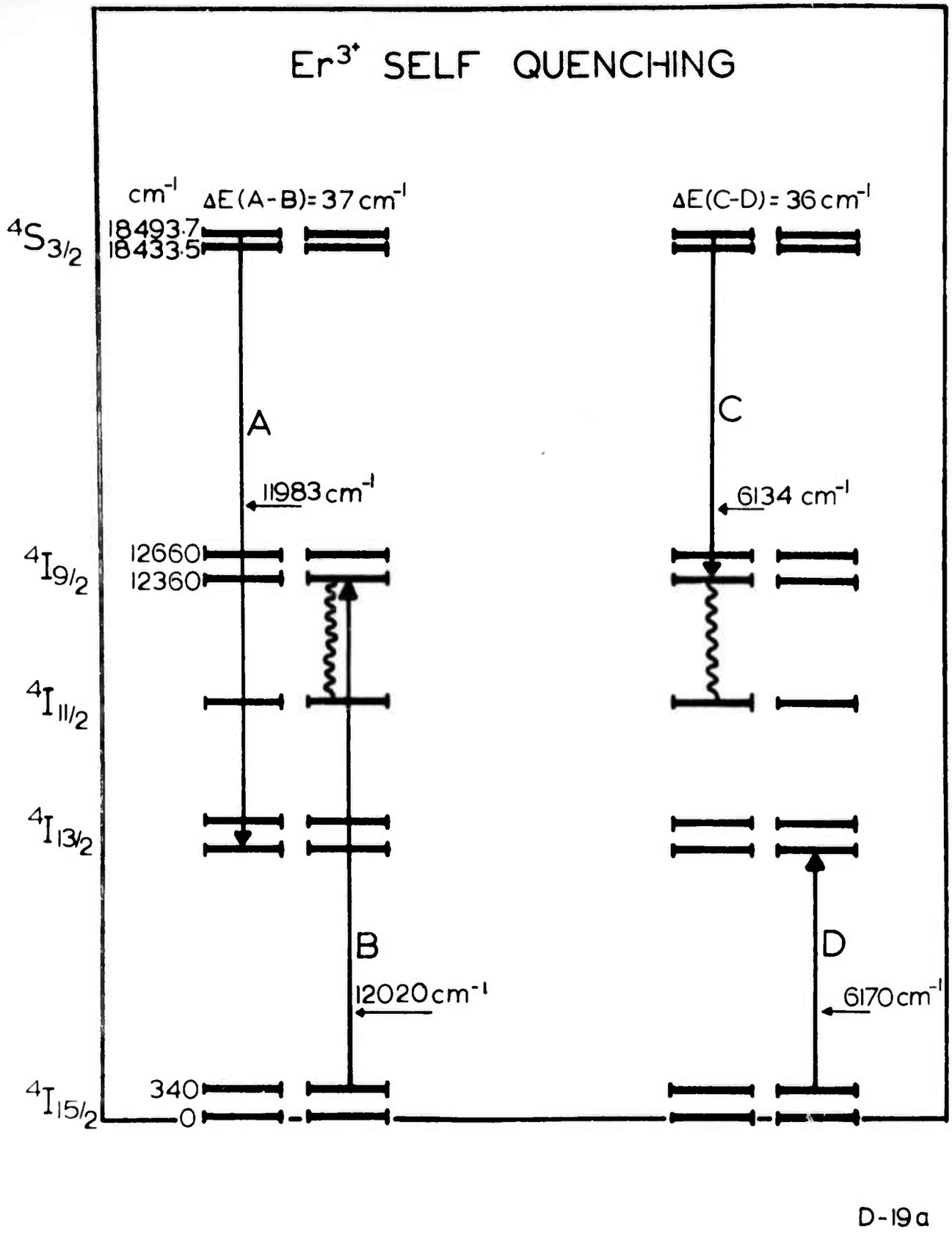

Figure 5-4 Er^{3+} Self Quenching.

The temperature dependence of the $^4S_{3/2}$ lifetime is largely the result of the temperature dependence of the occupation factors of higher lying states of the ground manifold expressed by

$$N^I = N \frac{e^{-E_L/kT}}{Z}$$

where

E_L = energy above the ground state of participating states ~340 cm^{-1}

Z = partition function of $^4I_{15/2}$

Thus the predicted temperature dependence of $\dot{N}$ is

$$\dot{N} = \frac{\omega N^S e^{-340/kT}}{Z}$$

neglecting the (weaker) temperature dependence of N^S.

5.2 $^4I_{13/2}$: THE TERMINAL LASER LEVEL

5.2.1 LEVEL ASSIGNMENTS

In S_4 symmetry $^4I_{13/2}$ (J = 13/2) is split into 7 Stark components.[20] Table 5-2 lists Brown's[17] measured (4.2°K) values of these states. The position of these levels at room temperature are presently being determined.

5.2.2 $^4I_{13/2}$ FLUORESCENCE LIFETIME

$^4I_{13/2}$ is some 6500 cm^{-1} above the ground state resulting in negligible non-radiative decay at least in dilute concentrations. The measured fluorescence lifetime is 13 ± 1.5 ms. In 100% Er samples ($LiErF_4$) the room temperature lifetime is 7 ± 1 ms.

TABLE 5-2

$^4I_{13/2}$ LEVELS (from Reference (17))

Identifying Notation	Wavelength (μm)	Energy (cm^{-1})	
A-1	1.53593	6510.7	
A-2	1.53515	6514.0	
A-3	1.52574	6554.1	
A-4	1.50426	6647.8	$\Delta E = 203.1\ cm^{-1}$
A-5	1.49897	6671.2	
A-6	1.49270	6699.2	
A-7	1.48946	6713.8	

5.3 PUMP BANDS

The pump bands for $^4S_{3/2}$ include, in principle, all Er^{3+} states above $^4S_{3/2}$ to the limit of host transparency ~0.15 μm. However, in order to provide useful pumping for laser operation, states must feed at a rate much faster than the $^4S_{3/2}$ lifetime[21] (200 μs in 2% Er).

In order to identify the useful pump bands, a 2% Er:YLF sample was selectively excited with a Xenon flash (pulse duration 20 μs) and the peak height and time of the $^4S_{3/2}$ emission detected. All the pump bands identified in table 5-3 feed $^4S_{3/2}$ sufficiently fast so that the fluorescence peak occurs <25 μs after the lamp trigger. At the present time it is not known whether states above $^4G_{11/2}$ contribute.

TABLE 5-3

Er:YLF PUMP BANDS

Sample 391: 2% Er:YLF

Central Wavelength[1] (μm)	Relative Amplitude[2] (mV)	Identification
0.518	80	$^2H_{11/2}$
0.490	60	$^4F_{7/2}$
0.483	150	$^4F_{5/2}$
0.447	50	$^4F_{3/2}$
0.403	30	$^2H_{9/2}$
0.375	55	$^4G_{11/2}$
0.360	25	$^4G_{11/2}$

[1] Exciting bandwidth ~50Å

[2] Amplitude of $^4S_{3/2}$ fluorescence at peak. Not corrected for source variations with λ.

5.4 TERMINAL STATE QUENCHING

Spectroscopic measurements were carried out using a number of Er:YLF samples co-doped with other RE^{3+} ions. The intent of these measurements was the determination of the appropriate composition which strongly quenches $^4I_{13/2}$ without quenching $^4S_{3/2}$.

5.4.1 Holmium (Ho^{3+})

The $^4I_{13/2}$(Er)-$^5I_7$(Ho) transfer (across a gap of ~800 cm^{-1}) results in a $^4I_{13/2}$ lifetime of 2 ms[18] with a corresponding rate of 433 sec^{-1} in 2% Er-2% Ho.

$^4S_{3/2}$ (Er) is also somewhat quenched in the presence of Ho^{3+} (lifetime 155μs). Faster rates out of $^4I_{13/2}$ can be obtained in higher concentrations - but at the expense of $^4S_{3/2}$. Ho^{3+} does not appear to provide an acceptable means of quenching $^4I_{13/2}$.

5.4.2 Terbium (Tb^{3+})

$^4I_{13/2}$ (Er^{3+})-$^7F_0$ (Tb) transfer across an energy gap of ~500 cm^{-1} occurs at a rate of ~470 sec^{-1} resulting in an observed 1.8 ms lifetime in 2% Er-2% Tb. $^4S_{3/2}$ was also quenched (lifetime 120 μs) eliminating Tb^{3+} from consideration.

5.4.3 Thulium (Tm^{3+})

The $^4I_{13/2}$ (Er)-$^3H_4$ (Tm) transfer occurs via the resonant process shown in figure 5-5. The indicated level positions, taken from low temperature absorption data,[13] are somewhat shifted and broadened at room temperature. As a result at room temperature the emission of $^4I_{13/2}$ overlaps the absorption of $^3H_4$ (i.e., the transfer indicated in figure 5-5 is resonant) and the transfer rate is very fast.

In Er-Tm crystals direct measurement of the $^4I_{13/2}$ lifetime by pulsed fluorescence could not be obtained accurately. This is due to the slow spontaneous rate of this manifold (~80 sec^{-1}) compared to the rapid non-radiative transfer (>500 sec^{-1}) to $^3H_4$ and the nearly overlapping (strong) Tm^{3+} fluorescence.

A reasonable estimate of the $^4I_{13/2}$ lifetime can be obtained from fluorescence spectra by determining the ratio of fluorescence amplitudes in a reference crystal (2% Er) to the sample (mixed crystal). This is possible in cases where the "sensitizer" does not appreciably alter the pumping rate of a reference state ($^4I_{11/2}$). $^4I_{11/2}$ is chosen as the reference level because it is only very weakly quenched in the presence of other rare earth ions (except for Yb^{3+}) even in moderate concentrations. Thus the $^4I_{13/2}$ lifetime of a mixed crystal can be obtained from a measurement of fluorescence amplitudes:

$$\tau_S = Q^{-1} \quad R \quad .$$

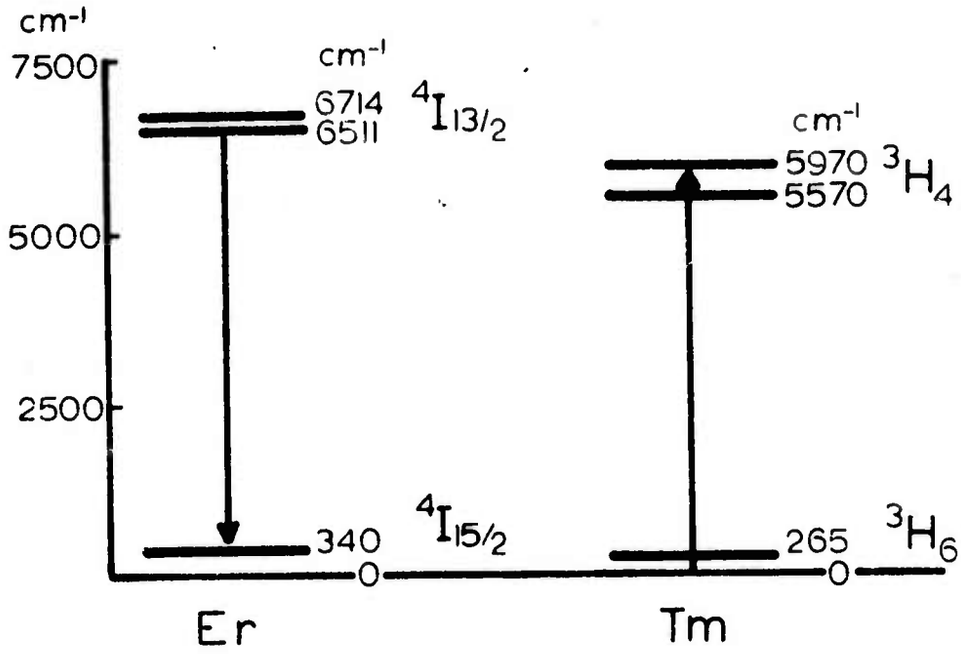

Figure 5-5 Er-Tm Resonant Transfer.

where

τ_R = $^4I_{13/2}$ lifetime of the reference sample (2% Er) = 13 ms

τ_S = $^4I_{13/2}$ lifetime of the mixed crystal

Q = quenching factor

In cases where the reference level ($^4I_{11/2}$) lifetime and pumping rate in the mixed crystal are independent of the quenching species Q can be obtained from

$$Q = \frac{A_R}{A_S}$$

where

A_R = fluorescence amplitude of $^4I_{13/2}$ in the reference crystal

A_S = fluorescence amplitude of $^4I_{13/2}$ in the mixed crystal

To account for differences in optical collection efficiency, scattering, etc, the amplitude data is normalized using the ratio of the $^4I_{11/2}$ amplitudes (corrected for lifetime variations) in the mixed and reference crystals. In this way the $^4I_{13/2}$ lifetime in the mixed crystal can be obtained to within the variation of the pumping rate of the respective states due to the "quenching" species (estimated less than a factor of 2).

Figures 5-6 through 5-8 show the emission spectra of 2%Er, 2% Er-1% Tm, 2% Er-2% Tm:YLF. Table 5-4 lists the quenching factors obtained from these data and the estimated lifetimes as well as the lifetimes of the $^4S_{3/2}$ manifold for these samples. Tm^{3+} in low concentrations (<2%) does promote very strong quenching of $^4I_{13/2}$. However, resonant transfer from Er-Tm initiating from $^4S_{3/2}$ (see figure 5-9) strongly quenches $^4S_{3/2}$ as well. Pr^{3+}, discussed below, appears to be considerably more favorable.

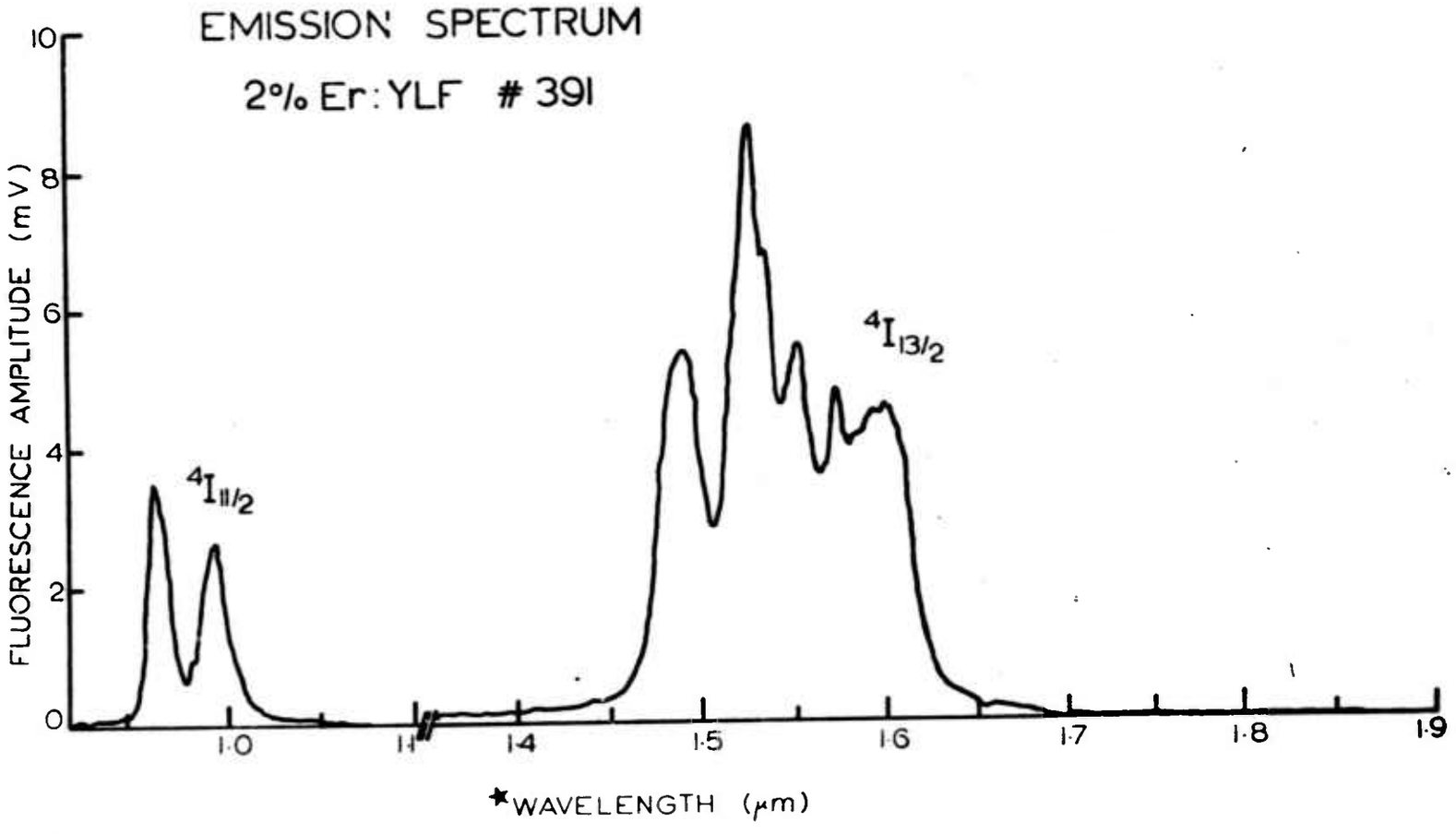

Figure 5-6 Emission Spectrum of 2% Er:YLF.

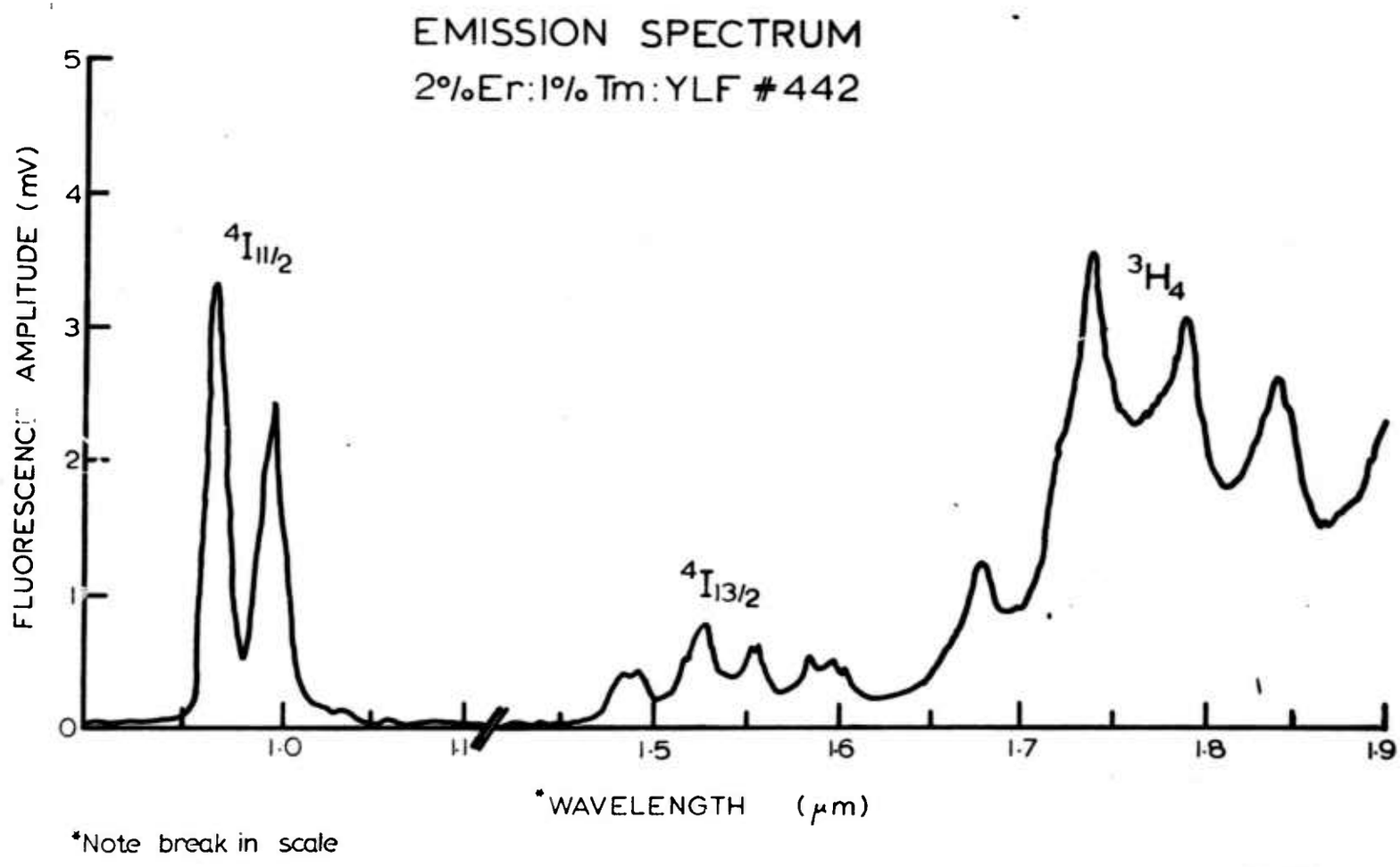

Figure 5-7 Emission Spectrum of 2% Er:1% Tm:YLF.

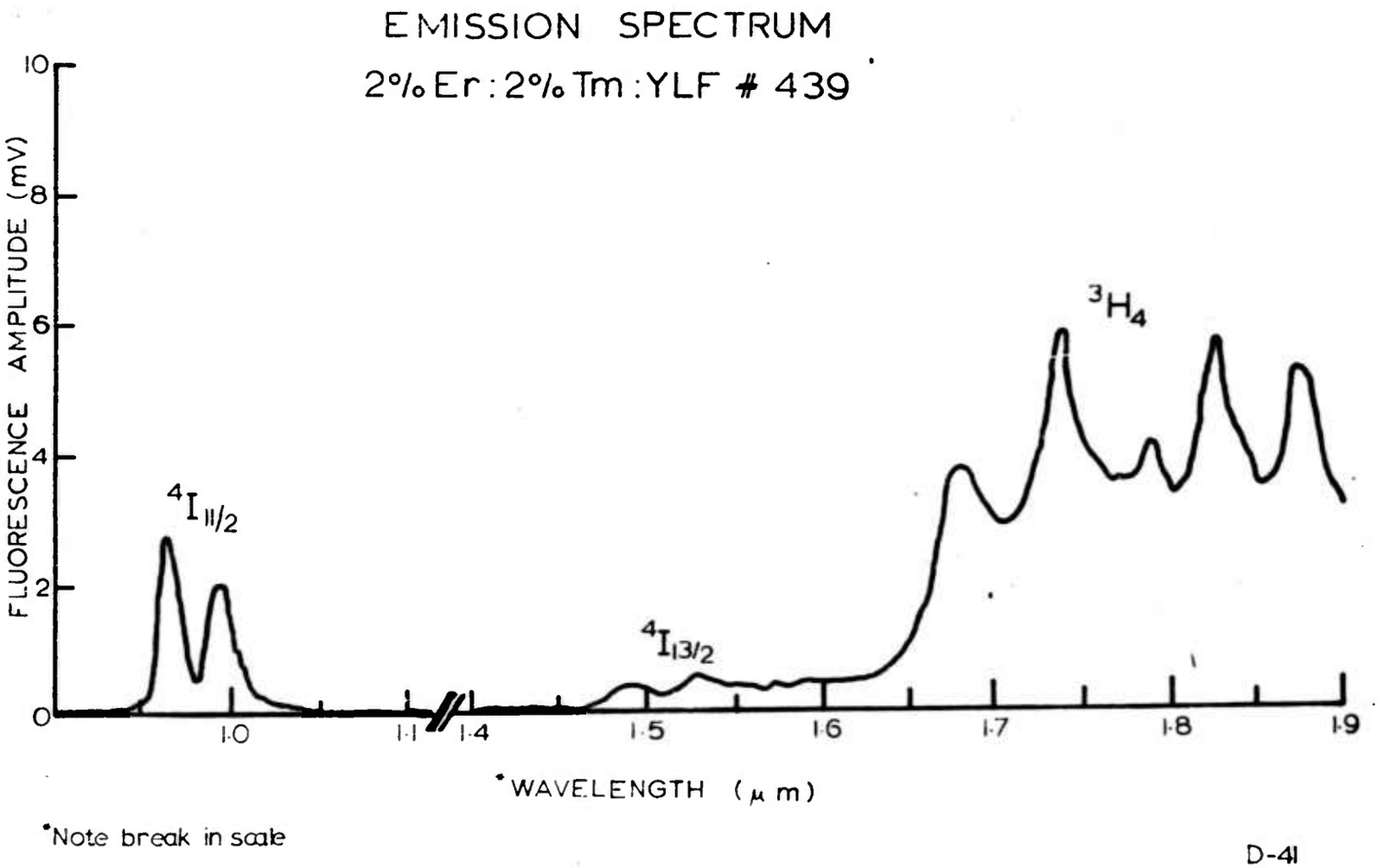

Figure 5-8 Emission Spectrum of 2% Er:2% Tm:YLF.

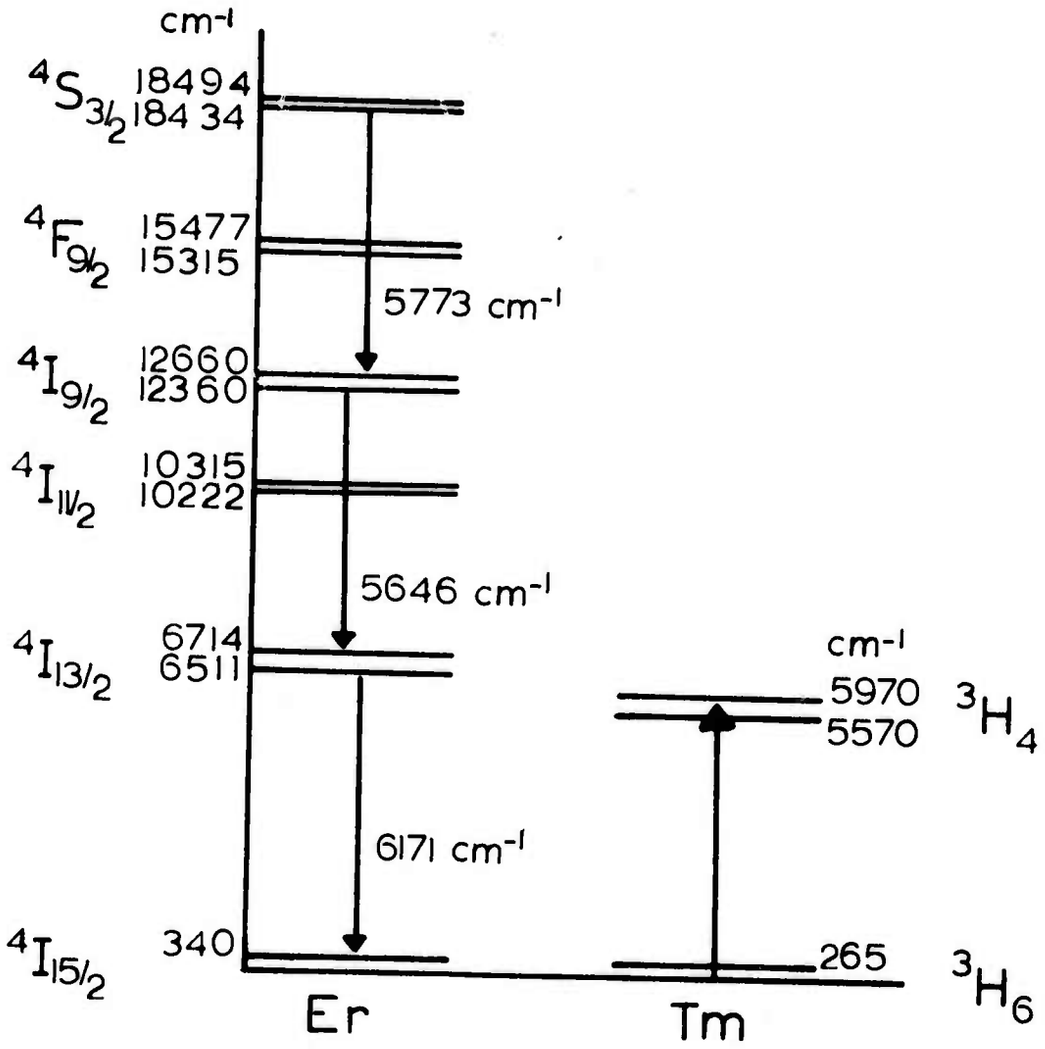

Figure 5-9 Accidental Resonances in Er-Tm:YLF.

TABLE 5-4

QUENCHING EFFECTS OF Tm^{3+} AND Pr^{3+}:YLF

Sample Number	Composition	Quenching Factor $^4I_{13/2}$	$^4I_{13/2}$ Lifetime	$^4S_{3/2}$ Lifetime
391	2% Er	--	13 ± 1 ms	200 ± 20 μs
442	2% Er-1% Tm	11	1.1 ms*	90 ± 20 μs
439	2% Er-2% Tm	18	0.7 ms*	70 ± 20 μs
444	2% Er-1% Pr	35	0.4 ms*	170 ± 20 μs
445	2% Er-2% Pr	50	0.25 ms*	110 ± 20 μs

* Inferred from fluorescence amplitude measurements, estimated accuracy to within a factor of 2.

5.4.4 Praeseodymium (Pr^{3+})

Samples of Er-Pr:YLF were grown to evaluate the $^4I_{13/2}$ (Er)-$^4I_{15/2}$ (Pr) transfer rate. Pr was chosen because there are no accidental resonances between ground state transitions in Pr with $^4S_{3/2}$ transitions in Er. Figures 5-10 and 5-11 show the emission spectra of 2% Er-1% Pr and 2% Er-2% Pr. Using figure 5-6 we obtain the estimated quenching factors and $^4I_{13/2}$ lifetimes which are tabulated in table 5-4.

Thus the most favorable composition examined to date appears to be 2% Er-1% Pr for repetitively pulsed operation. For 30 pps operation the interval between pulses is 33 ms. This time interval corresponds to some 33τ, i.e., $^4I_{13/2}$ will have decayed by a factor of exp (-33/0.4) between pulses. Thus saturation of the output due to population buildup in the terminal level between pulses can be neglected.

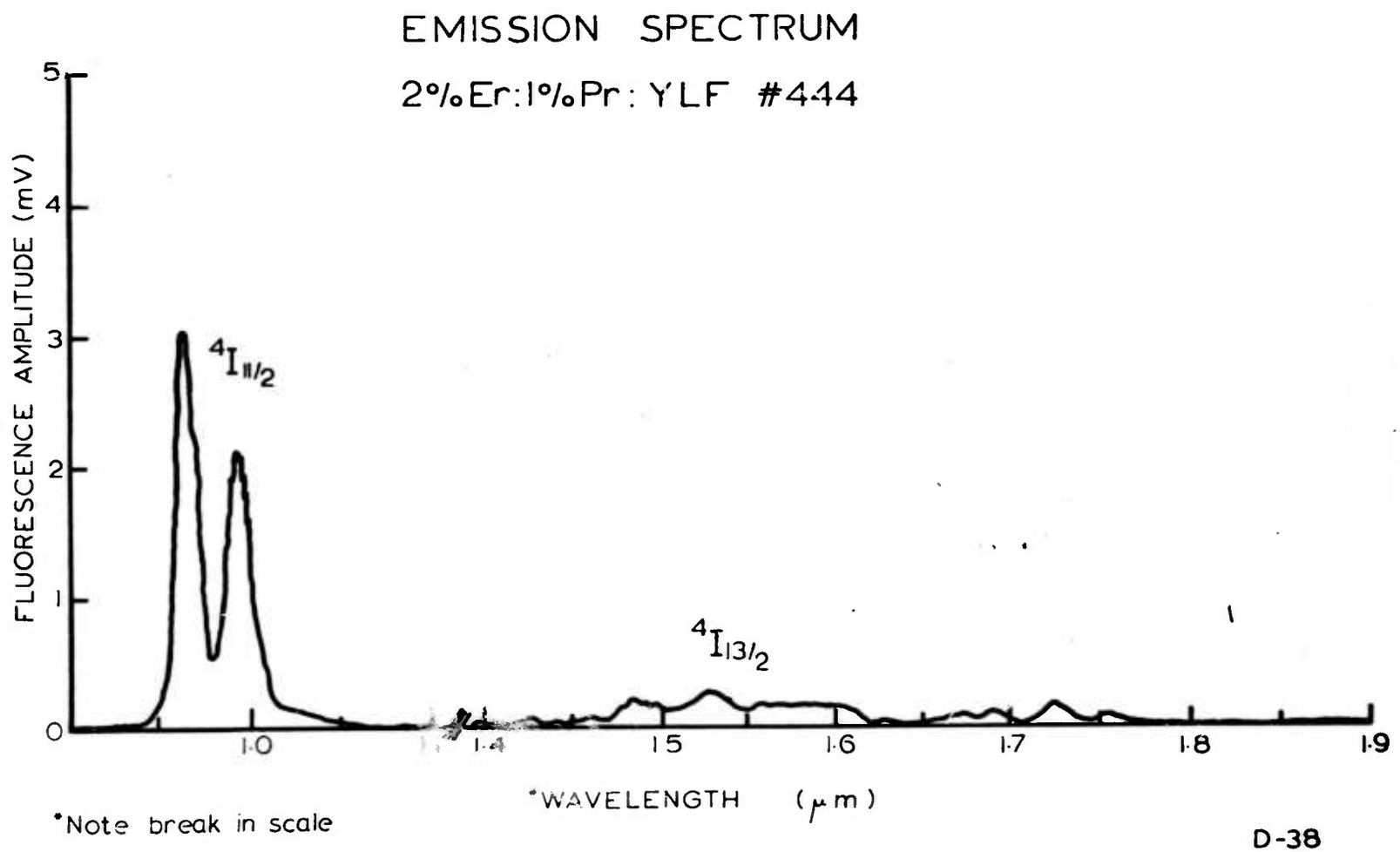

Figure 5-10 Emission Spectrum of 2% Er-1% Pr:YLF.

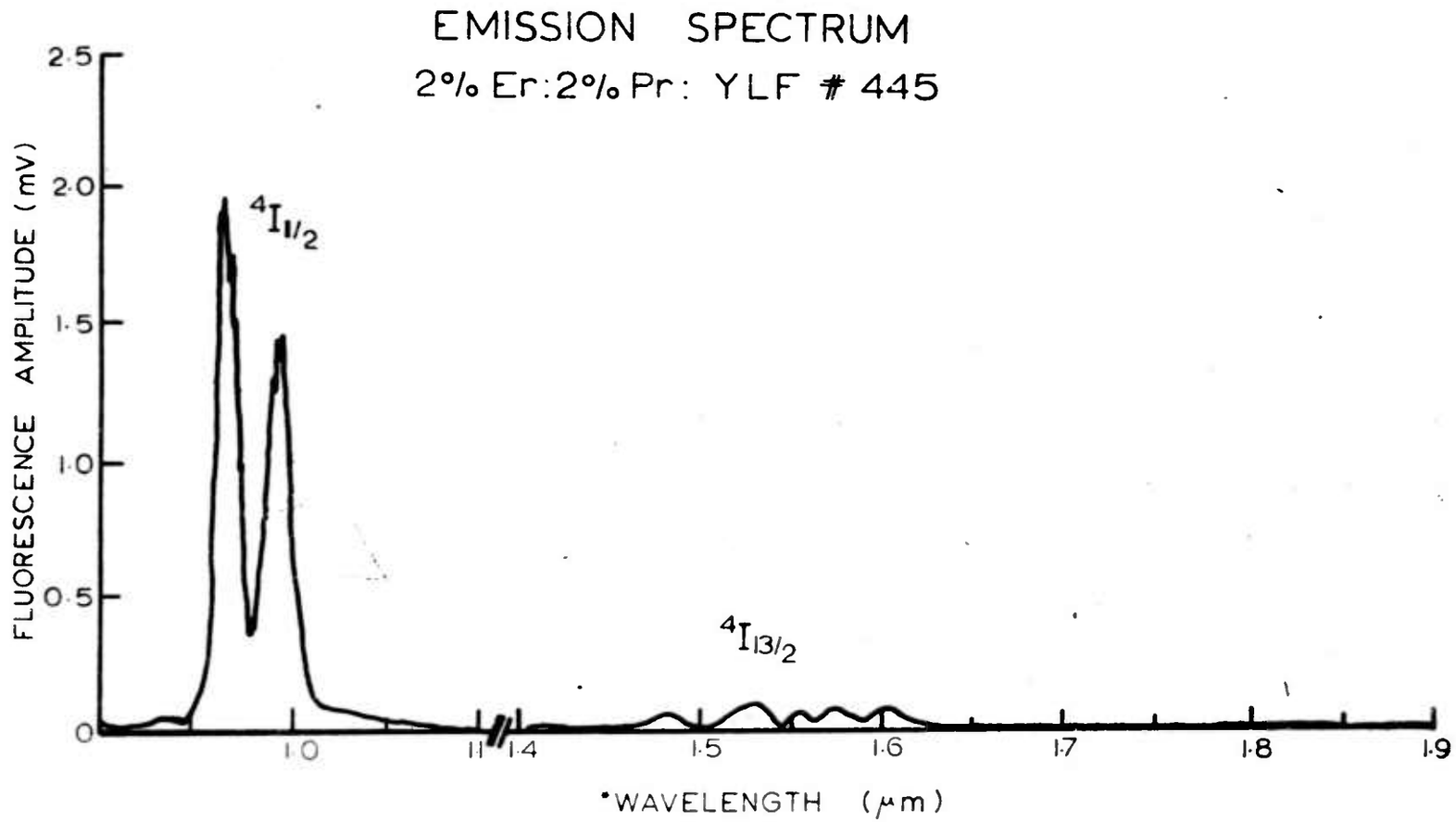

Figure 5-11 Emission Spectrum of 2% Er-2% Pr:YLF.

SECTION 6
LASER MEASUREMENTS

The primary emphasis during this phase of the program was to determine the effects of the operating parameters (flashlamp pulsewidth, fill pressure, output coupling, etc) on laser performance at room temperature. Most of the laser data were obtained using 2% Er:YLF rods. Limited testing of other compositions is reported; however, differences in the optical quality and size of different rods prevented unambiguous assignment of performance characteristics to specific compositional changes.

6.1 EXPERIMENTAL HARDWARE

6.1.1 PUMPING CAVITIES

Room temperature pulsed laser measurements were made in pumping cavities, the cross sectional dimensions of which are shown in figure 6-1. The reflective material is front surface silver which is prevented from tarnishing by continuously bleeding N_2 into the cavity during operation.

6.1.2 LASER ROD HOLDERS

Laser rod holders were designed for ease of mounting odd sized rods with minimal risk of breakage. Rods are glued onto split Spectrosil tubing (best glue: methyl-methacrylate dissolved in methylene chloride) and the tubing glued to the metal endcaps as shown in figure 6-1. One of the more serious experimental problems encountered during this work was the difficulty in maintaining optical alignment during the flashlamp discharge. The dynamic alignment is monitored by observing the relative motion between the Fresnel reflections off the rod and mirrors of the He-Ne alignment laser during the flashlamp discharge. For example, angular displacements (between the rod and mirrors) of up to ~1 degree are typically observed in an "insecure" laser head assembly at a flashlamp loading of 30 J/inch. In a secure assembly the alignment after the flashpulse is within the initial alignment accuracy (estimated: 0.005 degree). As yet a prescription

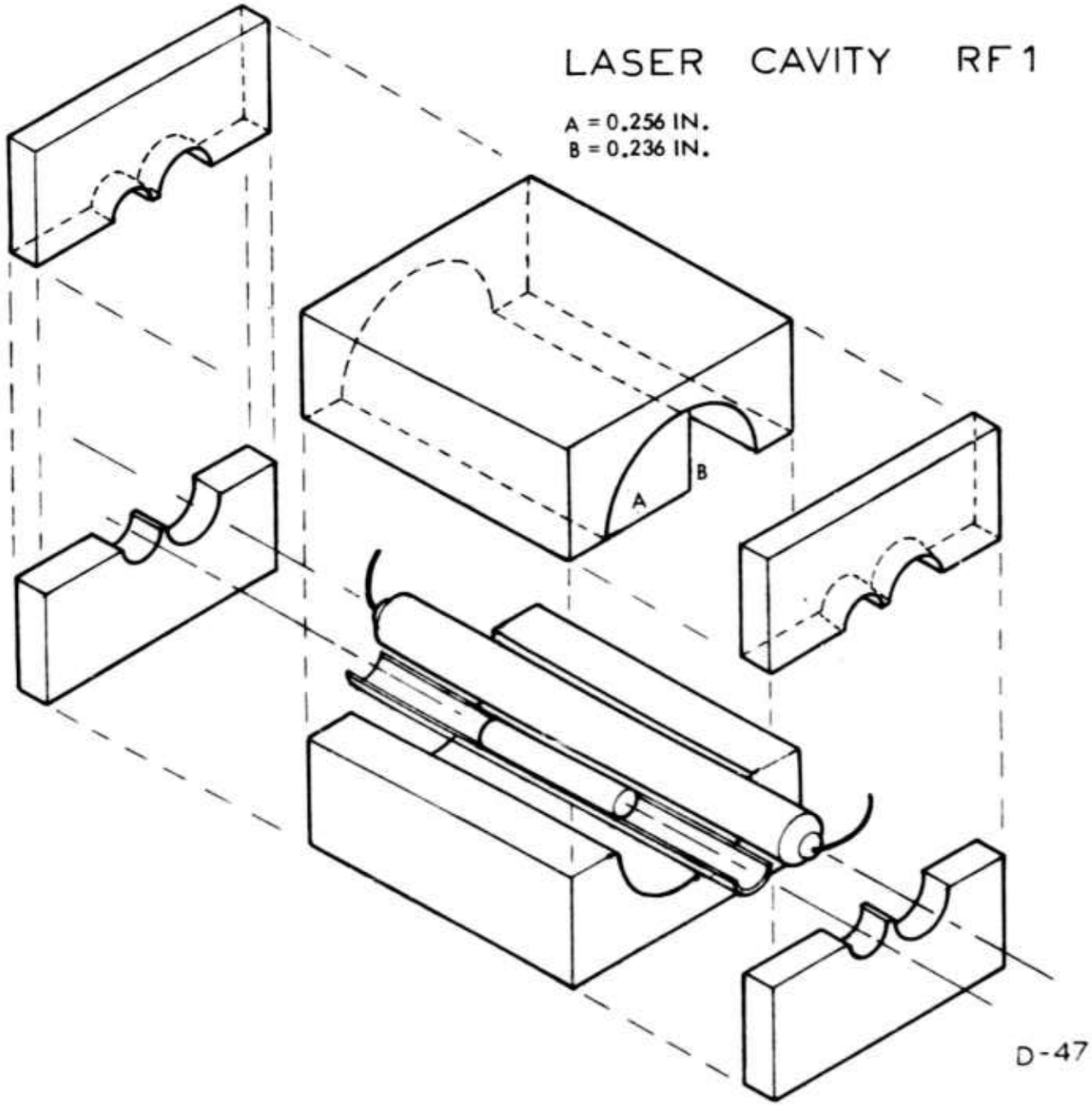

Figure 6-1 Laser Cavity.

for laser cavity assembly for eliminating rod motion is lacking, mounting integrity is obtained in a more or less trial and error fashion.

6.1.3 RESONANT CAVITY

Plane parallel dielectric reflectors were used for all measurements reported below. The mirrors are of fused silica with faces parallel to 2 arc seconds with the rear surface of the output mirrors AR coated at 0.85 μm. Rods were fabricated with flat/flat uncoated faces. One attempt at AR coating the rod surfaces was unsuccessful - both coatings damaged after only two shots (long pulse) at ~10 mJ output.

6.1.4 RADIOMETRY

Energy measurements were made with a TRG Model 102 Ballistic Thermopile. Simultaneously the spiking oscillation was recorded with various photodiodes viewing a portion of the output off a diffuse target.

6.2 LASER DATA

Table 6-1 describes a series of experiments in chronological order to determine the operating conditions for minimum threshold. Although the optimum values of each parameter were not carefully determined, a reduction in threshold by more than an order of magnitude was obtained by a combination of factors, the most important of which were: closer cavity coupling, flashlamp pulsewidth < fluorescence lifetime, higher fill pressure Xe lamps.

The use of higher current density discharges in a closely coupled cavity, however, has presented some problems. An input/output plot of rod 408 (measured before the start of this program) under pumping conditions described in line 1 of table 6-1 is shown in figure 6-2. The error bar indicates the estimated accuracy of the energy measurement; the variation from linearity of the experimental points shown may be due to alignment variations of the rod between slots as the rod was not mechanically secure in the pumping cavity. The data is presented to show that at ~2.5 × threshold, 150 mJ long pulses were obtained in contrast to the observed "saturation" discussed below.

TABLE 6-1

SUMMARY OF PREVIOUS RESULTS
2% Er^{3+}:YLF 0.85 μm
Room Temperature

Rod	Flashlamp (bore x arclength)	Pulsewidth FWHM	C/L	Pump Cavity	Threshold / Coupling Mirror
408 5x30mm	PEK Xe 14C-3 ~ 450 Torr 7mm x 3 in.	~ 250μs underdamped	375μF/stray	Front surface silvered cylinder d = 0.75"	105J[1]/20%T
408A 3 x 30mm	Xenon Corp. 2mm x 1.5" 200 Torr	160μs (overdamped)	50μF/130μH	Front surface silvered "ellipse" a = 0.33" b = 0.23"	30J/3%T
408A	Xenon Corp. 4mm x 1.5" 1000 Torr	~ 50μs	25μF/4μH	Second surface silver on quartz a = 0.33" b = 0.23"	16J/15%T
408A	Xenon Corp. 3mm x 1.5" 1000 Torr	70μs	25μF/70μH	Front surface silvered "ellipse" a = 0.33" b = 0.23"	8J[2]/3%T

[1] At ~ 3 x threshold (output: 158mJ) oscillations persisted for 250μs - oscillations started at 100μs after the trigger.

[2] Oscillations begin 70μs after flashlamp initiation. Flashlamp peaks at 80μs.

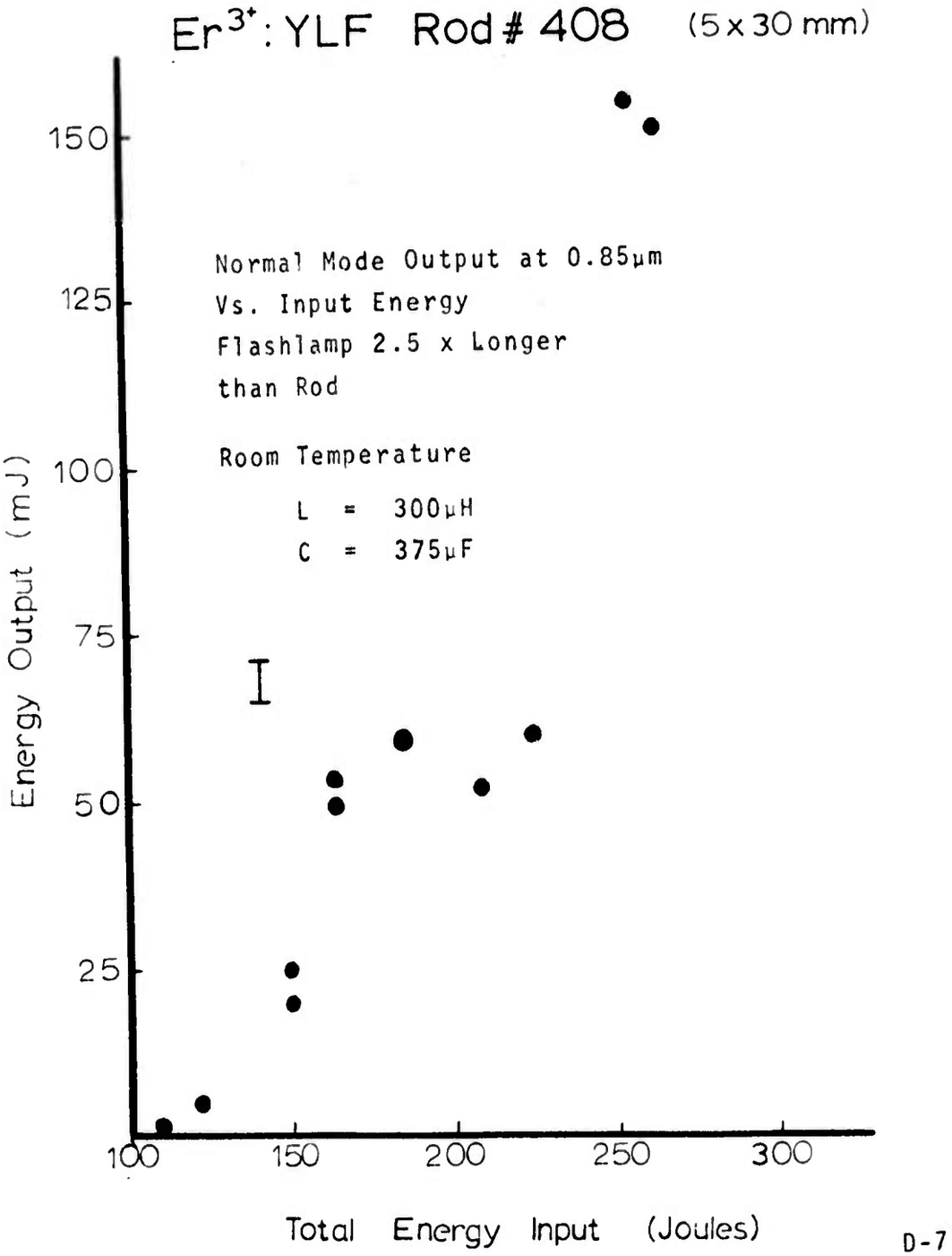

Figure 6-2 Energy Output vs. Input of Er:YLF Rod #408.

With the change in pumping conditions the threshold was dramatically reduced; however, in early measurements the output was observed to "saturate" at levels far below the energy outputs obtained in figure 6-2. This phenomenon was traced to rod motion induced, most likely, by the acoustic wave generated in the small pumping cavity by the flashlamp discharge.

With more careful attention to the mounting arrangement, the following long pulse data were obtained at room temperature. The experimental conditions were as follows.

Flashlamp: ILC 1200 Torr 3 × 30.5 mm

Storage Bank: C = 50 μF, L = 32 μH Single Mesh

Pulsewidth: 110 μs FWHM, Critically damped[22]

Resonator: Plane parallel with fused silica substrates - faces parallel to 2 arc sec, rear surface of output mirror is AR coated at 0.85 μm.

6.2.1 ROD 436.1: 2% Er-2% Ho (3 × 15 mm)

The spectroscopic lifetimes of this sample are:

$^4S_{3/2}$: 90 μs $^4I_{13/2}$: 3.1 ms

Lasing threshold for a rod of this composition (see figure 6-3) was only 7 Joules with the 30.5 mm arc length and 10 mJ output with 25J input. Above 20J input, difficulties were encountered in obtaining reproducible outputs. This is believed to be the result of rod motion.

6.2.2 408A: 2% Er ($^4S_{3/2}$: 200 μs, $^4I_{13/2}$: 13 ms) 3 × 27 mm

Despite the many bands of small bubbles throughout the volume of this rod, visible only under magnification, laser threshold for this rod was only 4 Joules under the same conditions described above (95% R output mirror). The results are presented in table 6-2 and figure 6-4. Reproducible data was not obtained

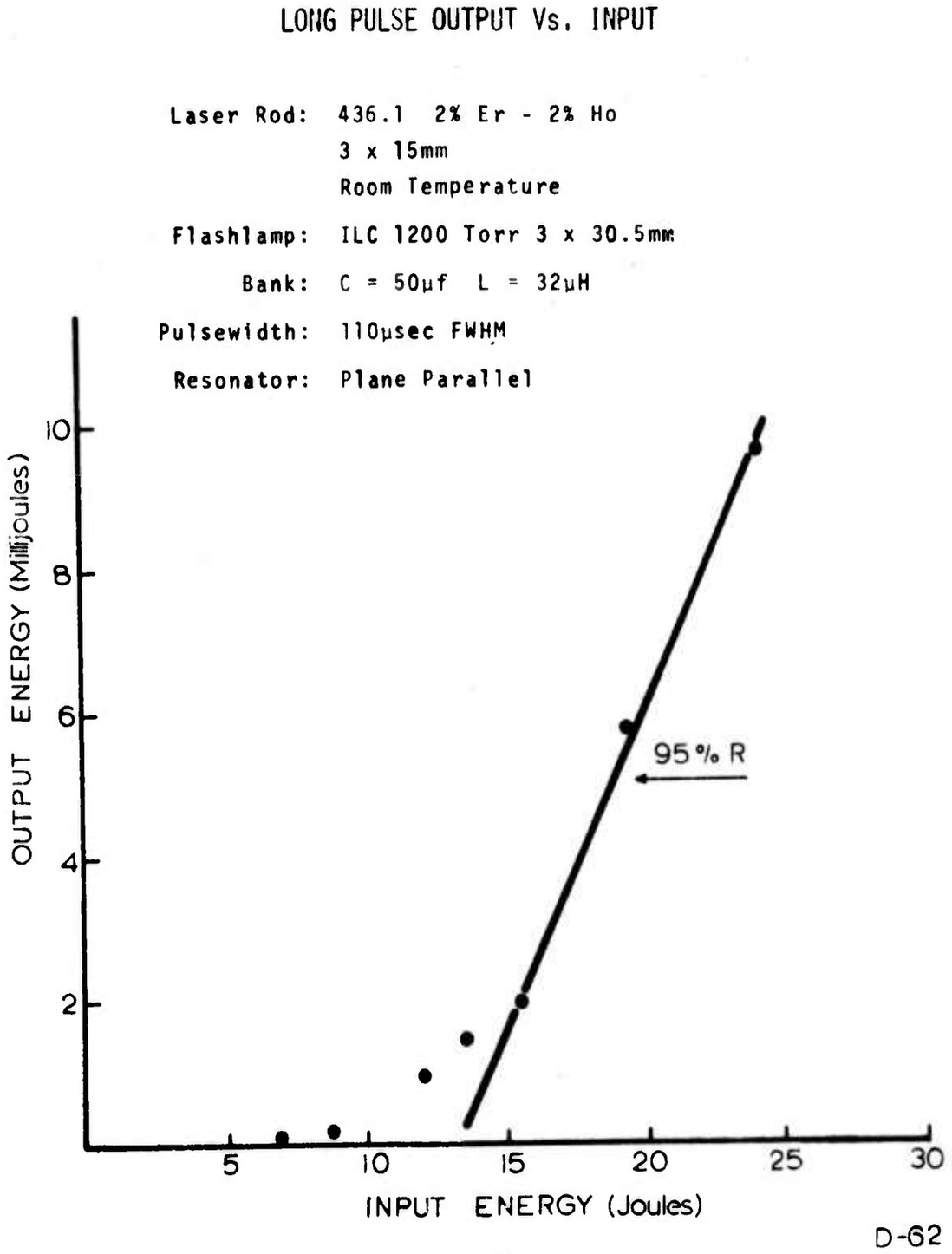

Figure 6-3 Energy Output vs. Input of 2% Er-2% Ho:YLF Rod #436.1.

TABLE 6-2

LONG PULSE INPUT/OUTPUT

Rod 408A: 3 × 27 mm 2% Er:YLF

C = 50 μF

L = 32 μH

1200 Torr Xe Lamp (3 × 30.5 mm)

Output Reflectivity	Threshold (Joules)	Input/Output
95%	4	25J/12mJ
85%	9	36J/13 mJ
70%	15.5	34J/29 mJ
50%	22	34J/12mJ

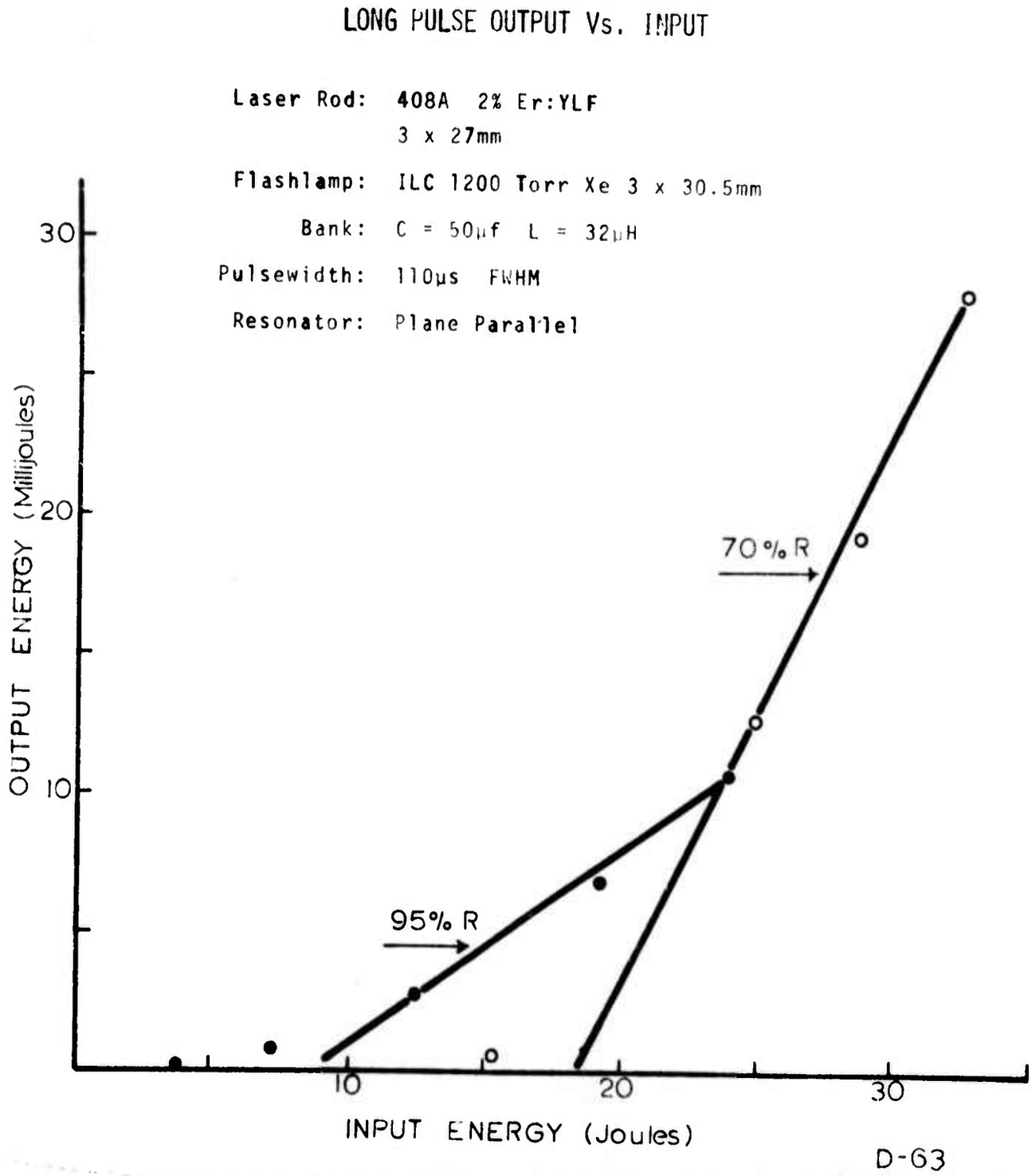

Figure 6-4 Energy Output vs. Input of 2% Er:YLF Rod #408A.

above ~35J input possibly due to rod motion mentioned above. For 95% and 85% R output mirrors, the maximum observed energy was 12 mJ; with 70% R the maximum 29J; and 50% R the maximum 12 mJ.

Previously a threshold of over twice this value, 9 Joules, was observed for this rod under nearly identical conditions (except L = 73 μH). The improvements in laser performance reported here reflect the combined effects of more stable rod mounting and improved cavity reflectivity.

6.2.3 ROD 437: 0.5% Er:YLF ($^4S_{3/2}$: 400 μs. $^4I_{13/2}$: 13 ms) 3 × 15 mm

This rod was of poor optical quality with two internal cracks obscuring approximately 1/5 of the cross section. Lasing threshold was approximately 9 Joules with only 1 mJ output at 20 Joules input. Above threshold the oscillation was characterized by irregular discrete spiking which persisted for up to 350 μs.

6.2.4 ROD 438.2: 2% Er:YLF 5 × 19 mm

Threshold for oscillation for this rod was 8 Joules with a 95% R coupling mirror. The input/output characteristics are shown in figure 6-5. With a somewhat longer pulsewidth (C = 100 μf, L = 73 μH, pulsewidth 200 μs FWHM) 46 mJ output for 30 Joules input with 95% R has been obtained.

6.2.5 ROD 438.1 (5 × 15 mm), EFFECTS OF PULSEWIDTH

Input/output measurements were made in the pumping described above with the pulsewidth varied by changing the C and L of the discharge circuit maintaining a critically damped condition. The experimental parameters were as follows:

Flashlamp: Xenon Corp. 5498C: 1200 Torr
3 mm bore × 25 mm arc

Storage Bank: C = 100 μf
L = 47 μh
} Pulsewidth: 140 μs FWHM

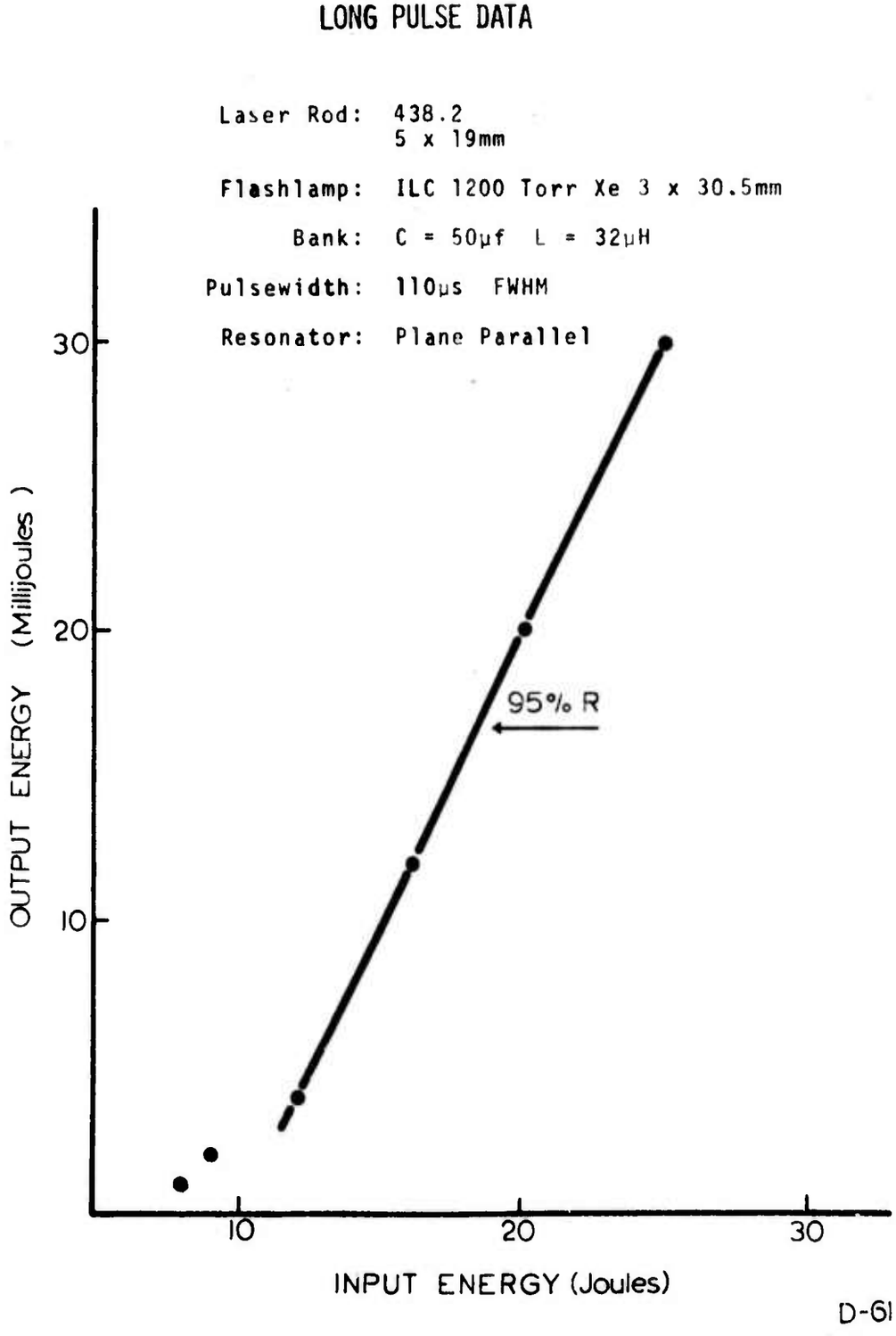

Figure 6-5 Energy Output vs. Input of 2% Er:YLF Rod #438.2.

C = 50 μf
L = 12 μh
} Pulsewidth: 60 μs FWHM

C = 25 μf
L = 3 μh
} Pulsewidth: 44 μs FWHM

Output Mirror: 97% R

The results are shown in figure 6-6 indicating increased overall efficiency with decreasing pulsewidth. Note that the variation of flashlamp radiative efficiency with current density (pulsewidth) has not been taken into account.

6.2.6 ROD 446.1

Long pulse measurements were made with rod 446.1: 2% Er, 5 × 67 mm at room temperature. The rod was of "good optical quality" except for a 1 cm region at one of the ends which exhibited large imperfections which appeared to be cracks. The pumping cavity was a front surface silvered cylinder of elliptical cross section: a = 0.33 in., b = 0.23 in., L = 50 mm. Only 50 mm of the rod length was pumped. The pumping conditions and input/output characteristics are shown in figure 6-7. The computed slope efficiency is 0.25% with 0.16% overall efficiency at 50J input. After about 50 shots the output fell drastically.

Upon removal it was found that the portion of the rod which was outside the cavity (the segment with the crack-like inclusion) had become almost opaque; i.e., the imperfections had become larger. Damage was not observed in the clear region of the rod. The rod was sent out for cutting and refabrication

6.2.7 ROD 408A (3 × 27 mm), REPETITIVELY PULSED OPERATION

Rod 408A (2% Er) was mounted in a water cooled cavity to investigate repetitively pulsed operation. The cavity was of cylindrical cross section (diameter 20 mm) of length 38 mm with a separation of 11 mm between rod and lamp centers. Cavity design was based on ease of mounting and removal of 3 mm rods with pumping efficiency an important but secondary consideration.

0.85 μm LONG PULSE INPUT/OUTPUT vs. PULSEWIDTH

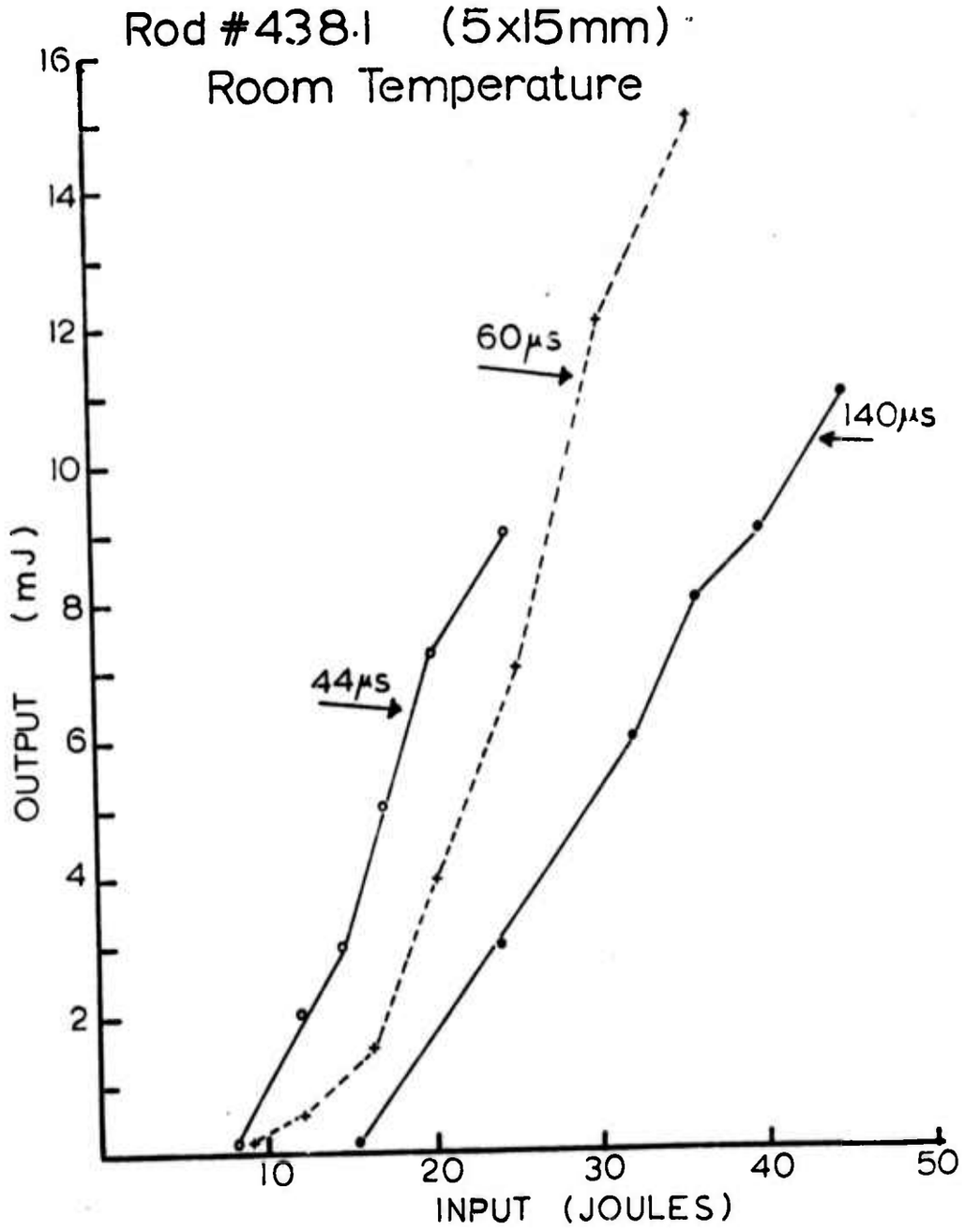

D-44

Figure 6-6 Input/Output vs. Pulsewidth.

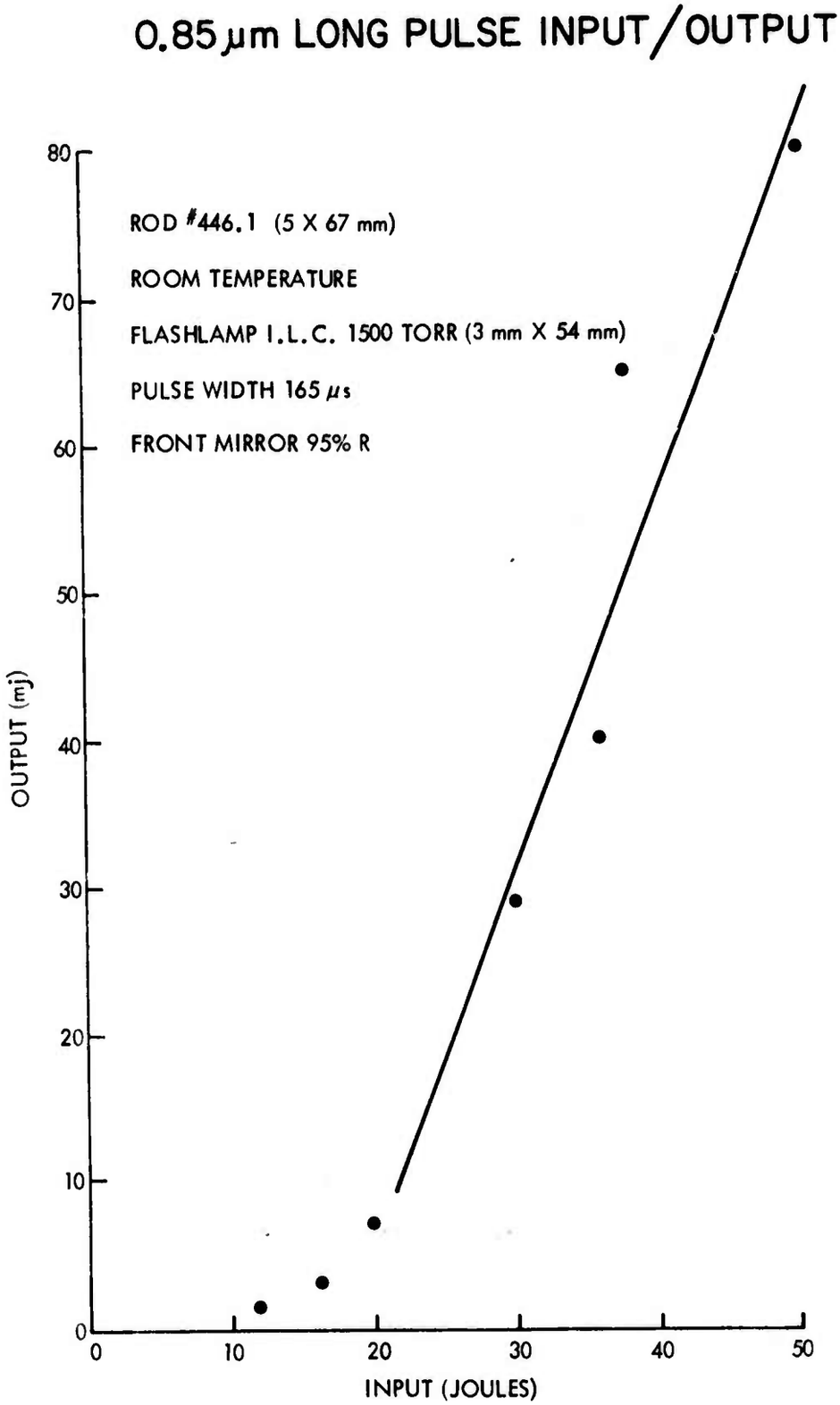

D 54

Figure 6-7 Energy Output vs. Input of 2% Er:YLF Rod #446.1.

The lamp was continuously simmered at 40 mA and the main bank (C = 50 μf, L = 90 μh) fired by triggering a series SCR with a pulse generator. Threshold in single shot was ~9 joules with a 3 × 25 mm 3000 torr Xe lamp. Long pulse operation was obtained at 10 pps with ~20J input/pulse. Oscillation was visually observed with a Varoscope. However, after 2-5 seconds oscillation ceased. Lasing was again observed (for ~3 seconds) after extinguishing the lamp for 10 seconds. This cycle was repeated ~20 times after which cavity tarnish lowered the pumping efficiency to the point where oscillations were not observed in single shot up to 25 joules input. Measurements of average power were not made. The source of this apparent quenching is not yet known.

6.3 MATERIAL DAMAGE

No evidence of internal damage has been observed in any Er:YLF rods. Before the start of this program, Q switched outputs up to ~0.5 MW (rod 408) had been obtained without any evidence of internal damage. Damage to laser rod faces, however, has been observed, even in long pulse operation. Surface damage has the appearance of small pit craters and may be the result of improper cleaning and/or flaws in the final optical polish.

Flashlamps fabricated from clear fused quartz and operated at high current densities are routinely used for pumping. Despite the high uv irradiance under such conditions, color center formation or other material artifacts have not been observed. Furthermore in pumping experiments conducted elsewhere with Tb^{3+}:YLF using dye laser flashlamps (up to 100 joules/inch in 1 μs), flashlamp induced damage was not observed.[23]

REFERENCES

(1) E. Snitzer and R. Woodcock, Appl. Phys. Lett. 6, 45 (1965)

(2) M. Robinson and D.P. Devor, Appl. Phys. Lett. 10, 167 (1967)

(3) Yu. K. Voronko, G.M. Zverev and A.M. Prokhorov, Sov. Phys. JEPT 21, 1023 (1965)

(4) M.J. Weber, M. Bass, G.A. DeMars, K. Andringa and R.R. Monchamp, IEEE J. Quantum Electronics QE-6, No. 10 (1970)

(5) R. Goldstein and F.N. Mastrup, IEEE J. Quantum Electronics QE-3, No. 11, 521 (1967)

(6) Yu. K. Voronko and V.A. Sychugov, Phys. Status Solidi 25, 119 (1968)

(7) E.P. Chicklis, C.S. Naiman and A. Linz, "Stimulated Emission at 0.85 μm in Er^{3+}-YLF", VII Int. Quant. Electr. Conference, Montreal (May 8, 1972)

(8) V. Belruss, J. Kalnajs, A. Linz and R.C. Folweiler, "Top Seeded Solution Growth of Oxide Crystals from Non-Stoichiometric Melts", Mat. Res. Bulletin 6, 899-906 (1971)

(9) Reactor Chemistry Division Annual Progress Report for Period Ending January 31, 1965, ORNL-3789

(10) R.E. Thoma, C.F. Weaver, H.A. Friedman, H. Insley, L.A. Harris and H.A. Yakel Jr., "Phase Equilibria in the System LiF-YF_3", J. Phys. Chem. 65, 1096 (1961)

(11) E.P. Chicklis, C.S. Naiman, R.C. Folweiler, A. Ling, H.P. Jenssen and D.R. Gabbe, "Development of Multiply Doped Ho:YLF as a Laser Material", Final Technical Report ECOM-0013F, ARPA Order 1868, Contract DAAB07-71-C-0013 (January 1973)

(12) Office of Naval Research, Contract N00014-67-A-0204-0044

(13) H.P. Jenssen, "Phonon Assisted Laser Transitions and Energy Transfer in Rare Earth Laser Crystals", Crystal Physics Laboratory Technical Report No. 16, Center for Material Sciences and Engineering, Mass. Inst. of Tech. (September 1971)

(14) G. Keller and H. Schmutz, J. Inorg. and Nucl. Chem. 27, 900 (1965)

(15) W.A. Shand, "Single Crystal Growth and Some Properties of $LiYF_4$", J. Crystal Growth 5, 143-146 (1969)

(16) J.R. Thornton, et al, Appl. Optics 8, 1087 (1969)

(17) M.R. Brown, K.G. Roots and W.A. Shand, J. Phys. C. (Solid State Phys.) Ser. 2, Vol. 2, 593 (1969)

(18) L.A. Riseberg, H.W. Moos and W.D. Partlow, IEEE J. Quant. Electr. QE-4, No. 10, 609 (1968)

(19) R.V. Bakradze, G.M. Zverev, G. Ya. Kolodnyi, G.P. Kuznetsova and A.M. Onishchenko, Soviet Physics-Solid State 9, 733 (1967)

(20) K. Patek, "Glass Lasers", CRC Press, p. 60 (1970)

(21) E.P. Chicklis and C.S. Naiman, Paper presented at First European Electro-Optics Markets and Technology Conference, Geneva, Switzerland (September 12, 1972)

(22) J.P. Markiewicz and J.L. Emmet, IEEE J. Quant. Electr. QE-7, No. 11 (1966)

(23) H.P. Jenssen, MIT, Work performed under ONR Contract N00014-67-A-0204-0044, "Blue-Green Laser Materials"

UNCLASSIFIED

Security Classification

DOCUMENT CONTROL DATA - R & D

(Security classification of title, body of abstract and indexing annotation must be entered when the overall report is classified)

1. ORIGINATING ACTIVITY (Corporate author) Sanders Associates, Inc. 95 Canal Street Nashua, New Hampshire 03060	2a. REPORT SECURITY CLASSIFICATION Unclassified 2b. GROUP N/A

3. REPORT TITLE

0.85 Micron Solid State Laser Material Evaluation

4. DESCRIPTIVE NOTES (Type of report and inclusive dates)

Semi-Annual Report, 5 June 1972-5 December 1972

5. AUTHOR(S) (First name, middle initial, last name)

Evan P. Chicklis, Robert C. Folweiler, Charles S. Naiman, et al

6. REPORT DATE	7a. TOTAL NO. OF PAGES	7b. NO. OF REFS
April 1973	76	23

8a. CONTRACT OR GRANT NO.	9a. ORIGINATOR'S REPORT NUMBER(S)
F33615-72-C-2065 b. PROJECT NO. 2075 c. d.	None 9b. OTHER REPORT NO(S) (Any other numbers that may be assigned this report) None

10. DISTRIBUTION STATEMENT

Distribution is limited to U.S. Government Agencies only by reason of inclusion of test and evaluation data; applied March 1973. Other requests for this document must be referred to AFAL/TEO, Wright-Patterson AFB, Ohio 45433.

11. SUPPLEMENTARY NOTES	12. SPONSORING MILITARY ACTIVITY
None	Advanced Research Projects Agency Materials Science Directorate 1400 Wilson Blvd., Arlington, Va. 22209

13. ABSTRACT

This first semi-annual report describes the current status of an investigation of Er:YLF as a 0.85 μm laser material operating at room temperature. Laser operation occurs via stimulated emission between the $^4S_{3/2}$-$^4S_{13/2}$ manifolds of the Er^{3+} ions. A description of the growth technique is presented. YLF crystals are grown by the Top Seeded Solution Technique, a modification of the Czochoralski process. A compendium of the physical properties of the host material is presented including crystal structure, hardness, thermal conductivity, density, thermal expansion, and modulus of elasticity. Pump bands for the laser transition (at least to 0.360 μm) rapidly feed $^4S_{3/2}$ at a rate much faster than the decay rate of this state: 200 μs in 2% Er. The terminal state ($^4I_{13/2}$) lifetime is 13 ms and is strongly quenched with the addition of Pr^{3+} without appreciably perturbing $^4S_{3/2}$. Room temperature laser data includes pulsed thresholds as low as 4 joules with slope efficiencies up to 0.25%. Repetitively pulsed operations at 10 pps is reported.

DD FORM 1 NOV 68 1473 REPLACES DD FORM 1473, 1 JAN 64, WHICH IS OBSOLETE FOR ARMY USE.

UNCLASSIFIED

Security Classification

14. KEY WORDS	LINK A		LINK B		LINK C	
	ROLE	WT	ROLE	WT	ROLE	WT
0.85 Micron Laser						
Laser Material Evaluation						
Er:YLF						
Erbium						
Stimulated Emission						
Top Seeded Solution Technique						
Four Level Laser						
Optically Pumped Laser						
Lithium Yttrium Fluoride						
YLF						
IR Laser						